INTERPRETATION OF ARCTIC BLACK CARBON MEASUREMENTS WITH A CHEMICAL TRANSPORT MODEL

by

Andrew Morrow

Submitted in partial fulfillment of the requirements
for the degree of Master of Science

at

Dalhousie University
Halifax, Nova Scotia
January 2015

Table of Contents

List of Tables

List of Figures

Abstract

Black carbon is a pollutant of concern in the Arctic; however models struggle to accurately simulate its seasonal cycle observed from in-situ measurements. This work aims to examine the contribution of different types of emissions from various regions to this cycle using the GEOS-Chem model. Base model emissions were modified by introducing a seasonal cycle on the existing emissions from domestic wood burning, and the addition of gas flaring emissions. To assess the efficacy of these changes, comparisons were made with ground measurements performed at Alert, Barrow, and Ny-Alesund, along with airborne measurements performed by the PAMARCMiP aircraft campaign. The best agreement was found at Alert and Barrow with the simulation using all modifications. The Ny-Alesund site, due to its elevation, had a different cycle than the one observed at the other sites which the model had difficulty in recreating. Vertical profiles obtained from PAMARCMiP showed good agreement, however the effects of the emissions changes diminished rapidly with altitude. Source regions of pollution in the model were assessed as well. The major source region at altitudes above the planetary boundary layer was found to be East Asia in the winter, spring and fall, while biomass burning was a major contributor during the summer. Closer to the ground, Europe and East Asia were the major contributors, with smaller contributions from North Asia and North America.

List of Abbreviations and Symbols Used

α	Angström Exponent
$\frac{g}{kg}$	Grams per kilogram
$\frac{m^2}{g}$	Meters squared per gram
$\frac{ng}{m^3}$	Nanograms per cubic meter
$\frac{W}{m^2}$	Watts per square meter
λ	Wavelength
μm	Micron
τ	Aerosol Optical Depth
b_{ext}	Extinction Coefficient
A	Area of soiled filter
AERONET	Aerosol Robotic Network
AGASP	Arctic Gas and Aerosol Sampling Program
AMS-SMPS	Aerosol Mass Spectrometer-Scanning Mobility Particle Sizer
AOD	Aerosol Optical Depth
ARCTAS	Arctic Research of the Composition of the Troposphere from Aircraft and Satellites

BC	Black Carbon
CALIPSO	Cloud-Aerosol Lidar and Infrared Pathfinder Satellite Observations
cm	Centimeter
ECHAM5-HAMMOZ	5th European Center for medium range weather forecasting Hamburg Model-Hamburg Aerosol Model-Model for Ozone and related chemical tracers
ECLIPSE	Evaluating the Climate and Air Quality Impacts of Shortlived Pollutants
FLEXPART	Flexible Particle dispersion model
GEM-AQ	Global Environmental Multiscale model with Air Quality processes
GEOS-Chem	Goddard Earth Observing System Chemical transport model
Gg	Gigagram
hPa	Hectopascal
I	Intensity
Int	Intercept
K	Kelvin
k	Specific Attenuation Coefficient

NASA	National Aeronautics and Space Administration
NETCARE	Network on Climate and Aerosols: Adressing Key Uncertainties in Remote Canadian Environments
nm	Nanometer
OC	Organic Carbon
PAMARCMiP	Polar Airborne Measurements and Arctic Regional Climate Model Simulation Project
PAS	Photoacoustic Spectrometer
POLARCAT	Polar Study using Aircraft, Remote Sensing, Surface Measurement and Models, of Climate, Chemistry, Aerosols, and Transport
Q	Rate of airflow through filter
R	Correlation coefficient
SO4	Sulphate
SP2	Single Particle Soot Photometer
SSa	Accumulation mode sea salt
SSc	Coarse mode sea salt
t	Time
z	Vertical Coordinate

Acknowledgements

This work would not have been possible without the support of Dr. Randall Martin and his research group, in particular Dr. Aaron Van Donkelaar, Dr. Betty Croft, and Colin Lee, members of the NETCARE network and numerous others who generously provided advice and data.

Chapter 1

Introduction

The Arctic is an environment that is vulnerable to human activity, affected by a changing climate to a larger degree than anywhere else. The Intergovernmental Panel on Climate Change predicts that for every degree that the global average temperature increases, the Arctic will see increases of double that or more through polar amplification (IPCC, 2013a). This warming is driving large scale change such as the increased rate of melting glaciers in Greenland. Between 1995 and 2005, the output from glaciers in Greenland more than doubled, from 90 to 220 cubic kilometers (Rignot and Kanagaratnam, 2006). Another widely publicized consequence is the loss of sea ice extent in the Arctic. The trend in September sea ice extent in the Arctic between 1979 and 2001 is -7% per decade, which increases up -14% per decade including 2013, with the 7 lowest values of September sea ice extent occurring within the last decade (Stroeve et al., 2014).

A major contributor to the changing climate is black carbon aerosols. They are a byproduct of inefficient combustion and a major pollutant in the Arctic, causing a global increase in forcing through all forcing mechanisms, including clouds and cryosphere forcing, estimated to be 1.1 $\frac{W}{m^2}$ with uncertainty bounds of 0.17 to 2.1 $\frac{W}{m^2}$ (Bond et al., 2013). These aerosols are transported from various source regions, sometimes as far south as 40 degrees north, a problem that is worsened in the winter and spring by slow removal processes and poor circulation (Stohl and Law, 2007), which causes an annual cycle for aerosols in the Arctic. The major removal process for carbonaceous aerosols is wet deposition, with 70-85 % of tropospheric aerosols

removed through this process (Pöschl, 2005). This process is slowed during winter in the Arctic due to the cold dry Arctic air, which has roughly one fifth of the water vapor that is found in the summer Arctic air (Serreze et al., 2012). This causes large differences in precipitation from summer to winter, for example at Alert in January, there is on average 9 cm of snow, compared to 20 cm of snow in July, along with 13 mm of rain (EC, 2010). Surface temperatures during the winter in the Arctic are low due to the absence of solar radiation for long periods of time, combined with a reflective surface of ice and snow. These low temperatures form stable inversions, which inhibits vertical transport and removal processes (Shaw, 1995). The combination of these two effects results in increased concentrations of aerosols and other pollutants during the winter and early spring.

Although they are sparse, a few stations in the Arctic and sub-Arctic measure black carbon aerosols and other pollutants. In addition to these ground monitoring stations, there have been various aircraft campaigns throughout the years which provide valuable data about pollutants higher in the atmosphere. One recent project which included Arctic aircraft flights was Arctic Research of the Composition of the Troposphere from Aircraft and Satellites (ARCTAS). These flights occurred in April, June, and July of 2008. The measurements collected during these flights have been analyzed to identify source regions for aerosol pollution during the spring and summer. One study performed using back trajectories concluded that the majority of measured black carbon in the lower troposphere was due to Russian biomass burning events, while Asian emissions dominated at higher altitudes (Matsui et al., 2011). These findings are consistent with other analysis of ARCTAS data with the GEOS-Chem chemical transport model (Wang et al., 2011). Another project involving Arctic flights that occurred during the same time period was the Polar Study using Aircraft, Remote Sensing, Surface Measurement and Models, of Climate, Chemistry, Aerosols,

and Transport (POLARCAT). Analysis of vertical profiles collected during flights in April in Alaska found enhancements in black carbon concentrations at altitudes of 4.5 km and 5.5 km, due to plumes from both anthropogenic sources as well as biomass burning plumes. Another study using POLARCAT data over Greenland along with FLEXPART modeling found that in air masses originating from North America, the pollution plumes contained far more sulphate than black carbon mass (Quennehen et al., 2011). The campaign that has been examined in this work is the Polar Airborne Measurements and Arctic Regional Climate Model Simulation Project (PAMARCMiP), which has performed flights Alaska and the Canadian Arctic in 2009, 2011 and 2012.

Although Arctic black carbon concentrations are still higher than in preindustrial times, they have fallen from maximum values measured in recent decades. Concentrations have decreased on average by 40% between 1990 to 2009 at three Arctic monitoring sites, Alert, Barrow, and Ny-Alesund (Sharma et al., 2013), and by as much as 80% aloft as measured by the AGASP (1983-1986) and PAMARCMiP (2009-2012) flight campaigns in northern Canada and Greenland (Stone et al., 2014). This decrease is thought to be mainly due to the decline in heavy industry after the collapse of the former Soviet Union (Sharma et al., 2004). There is concern about increasing pollution concentrations especially from gas flaring. A recent study found that while the practice of flaring waste gas contributed only 3% to the global BC emissions, north of 66 degrees gas flaring is the largest source of black carbon emissions. It contributes 66% of all black carbon emissions in the region, followed by biomass burning with 31%, with residential and other burning contributing only 3%. 42% of the annual mean black carbon surface concentration in the Arctic could be attributed to flaring (Stohl et al., 2013). This figure may increase as well, as a United States Geological Survey estimated that there are around 90 billion barrels of undiscovered,

technically recoverable oil (13 % of global amount) north of the Arctic circle, along with 40 billion barrels of proven oil (6% of global amount) (Robertson and Pierce, 2008).

These flaring emissions are included in a new emissions inventory compiled as part of Evaluating the Climate and Air Quality Impacts of Short Lived Pollutants (ECLIPSE), as well as recent global emissions for the years 2005 and 2010 (Kilmont et al., 2013). A modelling study investigating black carbon sources in Siberia using this inventory found better agreement with in-situ aircraft measurements than previous studies which did not include the flaring emissions (Raut et al., 2013). Another study using this inventory found that emitting black carbon in the Arctic will give almost a fivefold increase in the Arctic surface temperature response compared to emitting the same amount of black carbon at midlatitudes, due to the fact that a large amount of the black carbon emitted in the Arctic region remains in the lower part of the atmosphere and is deposited in the region (Sand et al., 2013). The ECLIPSE inventory was used in this work due to the fact that the black carbon emission inventory currently used in the GEOS-Chem model is out of date as it uses a base year of 2000 (Bond et al., 2007).

An approach to determining the source regions of Arctic black carbon is to perform a sensitivity study by perturbing emission in a chemical transport model. Past studies have identified that Asia is the main contributor to free tropospheric black carbon concentrations, and European, Russian, and North American sources dominate near the surface (Wang et al., 2011). This is broadly consistent with what has been found in a comparison of 17 different climate models (Shindell et al., 2008).

Broad scale source region studies have not taken into account Arctic gas flaring and the domestic heating cycle. These have been considered only in regional studies (Raut et al., 2013), or ones with very limited source regions (Arctic and mid-latitudes)

(Sand et al., 2013). The novelty of the work presented here is that it determines the contribution of gas flaring and domestic heating to Arctic black carbon, and takes it into account when determining source regions. These regions are also determined for all in-situ measurements including along the PAMARCMiP flight track, as well as for the entire Arctic region.

This document begins with an overview of aerosols and their effects on the environment, along with early research on aerosols in the Arctic in chapter 2. It then details various measurement techniques and campaigns that have occurred to monitor Arctic aerosols in chapter 3. The results of the work are presented in chapter 4, along with the conclusions that can be drawn from the results in chapter 5.

Chapter 2

Background

2.1 Aerosols and the Environment

The movement of energy in the atmosphere is a complex system, which can be affected to a large degree through human activity. The two main ways that this system is changed are the introduction of greenhouse gases and aerosols. While the effects of greenhouse gases are already fairly well documented and understood, the effects of aerosols are more uncertain (IPCC, 2013b).

Aerosols come from natural as well as anthropogenic sources. Natural aerosols include mineral dust entering the atmosphere when winds pass over desert regions, or sea salt entering the atmosphere from sea spray. Anthropogenic aerosols come mainly from combustion, the two main types being sulphate aerosols and carbonaceous aerosols (Jacob, 1999). Sulphate aerosols are strong scatters of visible light whereas black carbon aerosols absorb in the visible spectrum. Current figures for forcing due to aerosols are a global average of -0.6 $\frac{W}{m^2}$ to -0.2 $\frac{W}{m^2}$ for negative forcing due to sulphate aerosols and 0.05 $\frac{W}{m^2}$ to 0.80 $\frac{W}{m^2}$ for positive forcing due to black carbon aerosols (IPCC, 2013c). Aerosols can contain more than one component, especially if they have aged. This comes about through the condensation of various gases onto particles, and the coagulation of different types of particles (Heintzenburg, 1988).

Since these particles contain both scattering and absorbing components, it is useful to define the Single Scattering Albedo, which is the ratio of the scattering coefficient to the sum of the scattering coefficient and the absorption coefficient. This ratio

ranges from a value of 1 for a particle that is totally scattering to a theoretical limit of 0 for a particle that is totally absorbing, although in reality such a particle does not exist (Seinfeld and Pandis, 2006a). Another useful quantity in the study of aerosols is Aerosol Optical Depth (AOD). This is defined by the equation:

$$\tau = \int_{z_1}^{z_2} b_{ext}(z^{'}, \lambda)\mathrm{d}x \tag{2.1}$$

where τ is the AOD, z_1 and z_2 are the edges of a given thickness of the atmosphere, and b_{ext} is the extinction coefficient, which varies with both wavelength, λ, and height, $z^{'}$. The AOD appears in Beer's law:

$$I = I_o e^{-\tau} \tag{2.2}$$

where I is the intensity of a beam that has passed through a part of the atmosphere between the points z_1 and z_2, and I_o is the original intensity of the beam (Seinfeld and Pandis, 2006b). AOD calculated for the entire atmospheric column gives a useful measure of the total amount of aerosol above a given point. Since AOD is dependent upon the wavelength it is measured at, and not all instruments operate at the same wavelengths, one must use the Angström exponent in order to perform comparisons between instruments. The Angström exponent, which varies with wavelength (Kaskaoutis et al., 2007), is defined as

$$\alpha = -\frac{Log(\frac{\tau_{\lambda 1}}{\tau_{\lambda 2}})}{Log(\frac{\lambda 1}{\lambda 2})} \tag{2.3}$$

where $\tau_{\lambda 1}$ and $\tau_{\lambda 2}$ are known AODs at wavelengths $\lambda 1$ and $\lambda 2$. This is then used to calculate an unknown AOD using the equation

$$\tau_\lambda = \tau_{\lambda_o}(\frac{\lambda}{\lambda_o})^{-\alpha} \tag{2.4}$$

where τ_{λ_0} is a known AOD measured at wavelength λ_0, τ_λ is the AOD of interest that corresponds to the wavelength λ and α is the Angström exponent (Liou, 2002).

Both natural and anthropogenic aerosols can be grouped into two categories, primary and secondary aerosols. Primary aerosols are ones that are emitted directly into the atmosphere as particles, such as mineral dust, whereas secondary aerosols begin as gases and subsequently form aerosols. In general, primary aerosols tend to be larger and secondary aerosols tend to be smaller (Seinfeld and Pandis, 2006c).

The effects of these particles can be classified into direct and indirect effects. A direct effect is when incoming or outgoing radiation interacts with an aerosol through scattering or absorption. An indirect effect is when the presence of aerosols affects another natural process which interacts with radiation. For example if the atmosphere becomes supersaturated, water vapor will begin to condense onto aerosols and they will form cloud droplets. This mechanism is governed by the Kohler equation, which depends on the size and composition of a given particle. A smaller particle requires a higher super saturation than a larger particle of the same composition. Cloud droplets in a high enough concentration can reflect incoming radiation, or absorb outgoing radiation, depending upon their location and properties (Petty, 2006).

Aerosols are removed from the atmosphere in several ways. They can be scavenged by raindrops, ice, and snow as they fall out of the atmosphere, they can serve as cloud condensation nuclei or ice nuclei which will fall out of the atmosphere, or they can simply deposit out of the atmosphere. Smaller aerosols are generally only scavenged by precipitation, and larger particles can be scavenged, or simply sediment out of the atmosphere. This gives an average atmospheric lifetime of 3 to 10 days, which is long enough for aerosols emitted in Europe, Russia, and occasionally Asia to be transported into the Arctic (Bourgeois and Bey, 2011). Once these aerosols have ended up in the Arctic, it is the absorbing part of the aerosol that has a large effect on the local environment. This is due to the fact that the Arctic already has

a high albedo due to reflective snow and ice, therefore reflective sulphate aerosols do not much change the radiative balance. On the other hand black carbon aerosols heat the atmosphere while they are airborne, and then once they have deposited onto the snow or sea ice the albedo of the snow or ice is reduced, leading to increased melting. This effect is compounded when bare ground and open ocean is exposed by the decreasing snow cover, further decreasing the overall albedo of the ground which leads to even more warming (Quinn et al., 2011).

Black carbon is defined by four different physical properties, it absorbs strongly across all visible wavelengths with a mass absorption coefficient (the linear absorption coefficient divided by density) of at least 5 $\frac{m^2}{g}$ at a wavelength of 550 nm, it is composed of graphitic SP2 bonded carbon, it is refractory with a vaporization temperature near 4000K, and it is insoluble in water and common organic solvents (Bond et al., 2013). There are different methods to measure the black carbon mass of a given aerosol particle that exploit these physical properties, each with their own name. Elemental carbon refers to black carbon that has been captured on filters which are then heated to the point that the trapped particles begin to vaporize. The mass is calculated from reflected and transmitted laser light through the sample. Equivalent black carbon refers to black carbon that has been trapped on a filter and measured by comparing the transmission of light through a clean filter versus through a soiled filter. Refractory black carbon refers to black carbon that is measured by illuminating aerosol particles with a laser until they begin to vaporize and give off light, which can be measured. The measurements that these methods produce are not always equivalent. In general equivalent black carbon is the highest as it assumes that all light attenuation through the soiled filter is black carbon when in reality other substances can absorb as well. Elemental carbon is in the middle, and refractory black carbon is the smallest due to the fact that this measurement technique in its current form can only be performed on particles ranging from 70 to 500 nm (Lack et al., 2013).

One of the major Arctic sources of black carbon that is discussed in this work is black carbon from flaring. This is a process that occurs both at oil wells and petroleum refining facilities where natural gas that cannot be used is burned, usually on top of a high tower. Like any combustion process, one of the byproducts is black carbon. Although the burning of natural gas is relatively clean in comparison to some other fuel types, producing 0.77 grams of black carbon per kilogram of gas (McEwen and Johnson, 2012) as compared to 3.05 g/kg for bituminous coal (Chen et al., 2009), there are large volumes being burned in close proximity to the Arctic. Another factor that is explored is a seasonal cycle of emissions. The main contributor to this seasonal change in emissions is the burning of various types of fuels for heat during the winter. In China coal is still used as a heating fuel in many cities during the heating season from November until March. For example in the city of Xian in Northern China, 58% of the coal that is consumed is used for heating during this period (Cao et al., 2007). Changes in demand on the electrical grid that that requires more fuel to be burned to generate electricity contribute to this cycle as well. The electrical cycle is somewhat different though, peaking in the summer due to increased air conditioning use. The United States, which currently generates the majority of its electricity from combustibles, used 20% more electricity than an average month during July and August of 2012 (EIA, 2014). These cycles are important as transportation pathways change throughout the year due to meteorological changes, so to be able to understand seasonal pollution cycles in remote regions, an accurate temporal distribution of emissions is required.

2.2 Early Efforts

There has been interest in the study of black carbon for many years, dating from the mid-20th century. Early interest was spurred not by a changing climate, but by severe pollution episodes in England that were linked to higher rates of mortality

(Wilkins, 1954). The study of black carbon in the Arctic came about from interest in the phenomenon known as Arctic Haze. This term is used to describe the annual cycle of pollution in the Arctic, which reaches a peak in the late winter and early spring. These conditions were first noticed by whalers in the mid-18th century; however they owe their name to United States Air Force officer Murray Mitchell who did pioneering work in the study of the Arctic atmosphere (Mitchell, 1957). This cycle occurs due to several reasons. First of all in the winter there is a strong temperature inversion which limits vertical motion, trapping pollutants in the lower troposphere. There is also very little precipitation of any kind to remove particles from the air, and weather patterns during this time favor transport to the Arctic (Law and Stohl, 2007).

High concentrations of black carbon were first observed during a study done in Barrow in 1979, where concentrations were found to be at a similar level to some urban environments (Rosen et al., 1980). Around the same time, another group using data from Barrow found proof that this pollution originated from outside the Arctic (Rahn and McCaffery, 1980). High concentrations of vanadium were found during the winter high of Arctic Haze, which come from the burning of residual oil. This type of oil is too viscous to be used at temperatures found in the Arctic, so it is only burned in a temperate environment (Zoller et al., 1973). They concluded that this air most likely came from Europe, passing over Russia on its way into the Arctic. Efforts were made to understand the effect of this black carbon in the atmosphere, such as obtaining vertical profiles of black carbon concentrations over various places in the Arctic (Hansen et al., 1984). These measurements revealed that there were significant amounts of black carbon even at high altitudes. Calculations done at the time using similar conditions to what had been measured in these profiles (Cess, 1983) found that the change in the surface-atmosphere energy absorption at the top of the atmosphere averaged over 1982 was approximately 2.5 $\frac{W}{m^2}$. Another study that measured the amount of black carbon in Arctic ice and snow (Clarke and Noone,

1985) found that deposition onto the snow and ice was causing a reduction in albedo of 5 to 10 percent, which corresponded to roughly 3 $\frac{W}{m^2}$ of additional heating at the surface.

Although this work indicated that black carbon was present in large quantities in an otherwise pristine environment, and that it could be having a large effect on the exchange of energy in that environment, very little work was done to understand the role of black carbon in the Arctic over the next decade or so. Most work was focused on the effects of sulphate, as this was thought to be the major component of combustion related aerosols. For example, several early modeling studies (Charlson et al., 1992) (Schwartz, 1996) modeled their aerosols as purely scattering, with a single scattering albedo of 1. A subsequent study (Hegg et al., 1997) found that in fact a significant amount of the mass of small aerosols was in fact black carbon, and a more realistic single scattering albedo would be around 0.9.

Chapter 3

Monitoring the Arctic

Scientific measurements in the Arctic present a unique set of challenges due to the fact that much of it is very inaccessible, and the weather and temperatures are often extreme.

3.1 Arctic Black Carbon Monitoring Sites

Several Arctic sites monitor various chemical species, including black carbon and carbon monoxide. Carbon monoxide is also of interest as it is produced along with black carbon, so it can be used as a tracer for the transport mechanisms in the model (Pommier et al., 2010). The stations used in this work are Alert, Barrow, and Ny-Alesund, whose locations are presented in figure 3.2. The sites that measure black carbon use an Aethalometer produced by Magee instruments. This model of Aethalometer functions by drawing air over a quartz filter, trapping aerosols. The filter is illuminated with visible light, which is measured on the other side of the filter by two photo-diodes, one which measures the part of the filter which has been exposed to the aerosols, and one which measures a clean part (Hansen, 2005). The change in attenuation of light through the soiled part of the filter versus the clean part of the filter is collected over a period of time, and the black carbon concentration ($\frac{ng}{m^3}$) is determined using the following formula

$$BC = \frac{-100ALog(\frac{I_2}{I_1})}{kQ(t_2 - t_1)} \tag{3.1}$$

where A is the area of the soiled part of the filter, $\frac{I_2}{I_1}$ is the ratio of the intensities of the sample beam to the reference beam at times t_1 and t_2, Q is the flow rate of air through the filter, and k is the specific attenuation coefficient, which is recommended to be determined on a site by site basis as it can vary. The manufacturer suggests using a value of 19 $\frac{m^2}{g}$, which was found to be adequate at Alert and Barrow (Sharma et al., 2004). The Ny-Alesund site required a slightly lower specific attenuation coefficient of 15.9 $\frac{m^2}{g}$ (Eleftheriadis et al., 2009). These values must occasionally be adjusted, for example during the non-haze period from May until October at Alert a k value of 28.5 $\frac{m^2}{g}$ was found to be more appropriate. The different k values are necessary due to the different compositions of aerosols at each site, such as local dust contamination at Alert during the summer, and Ny-Alesund's elevation exposing it to different air masses. These measurements compare well with other measurement methods, with a an r^2 value of 0.91 and a slope of 0.95 when compared against Particle Soot Absorption Photometer measurements, and an r^2 value of 0.83 and a slope of 0.95 when compared against thermal black carbon measurements (Sharma et al., 2002). The detection limit of the Aethalometer is reported by the manufacturer as 100 $\frac{ng}{m^3}$ for an integration period of 1 minute (Magee, 2010), which drops to 15 $\frac{ng}{m^3}$ for a 30 minute integration period (Sandradewi et al., 2008), and down to 1.5 $\frac{ng}{m^3}$ for a 1 hour collection period (Polissar et al., 2001). The collection periods at the sites used were 5 minutes at Barrow, 30 minutes at Ny-Alesund and 60 minutes at Alert. The longer integration times at Alert and Ny-Alesund allow for a lower detection limit, wheras the short integration time at Barrow allows for more precise filtering of local pollution events due to its poximity to a population center, which is upwind of the station 24% of the time (Bodhaine, 1995).

Different methods of measuring black carbon can produce different concentrations, even if the measurements are taken at the same sites. This can be seen in figure 3.1,

which shows black carbon concentrations measured using both an aethalometer and weekly filter measurements. Both methods have various weaknesses that must be taken into account. An aethalometer assumes that all of the absorption that it has measured is due to black carbon, but other species of aerosol can contribute a small amount as well, leading to some over prediction. On the other hand, the filter method collects aerosol over the entire week, which means that it is difficult to filter out local pollution episodes. This causes an over prediction during the summer months when there are more local pollution sources, which can be filtered out of the aethalometer data due to its higher time resolution.

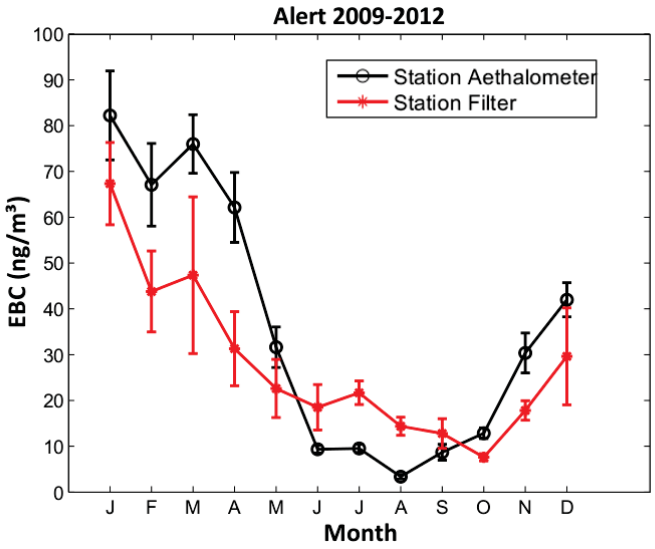

Figure 3.1: Comparison of filter and aethalometer black carbon measurements taken at Alert.

Sites collecting carbon monoxide data use a variety of different instruments, however they all operate on roughly the same principle. Carbon monoxide will absorb ultraviolet light, and then fluoresce in the visible range, at a wavelengths of 450 nm, 480 nm, and 520 nm (Carrivain and Orain, 2013) . The amount of carbon monoxide is calculated from the intensity of the fluorescence, or the amount of absorption (ESRL,

2014). In some cases the carbon monoxide is reacted with mercuric oxide, and it is the resulting mercury gas that absorbs (SRI, 2014).

3.2 Aircraft Campaigns

The PAMARCMiP campaign was selected for this work due to the fact that it has data from multiple years. This campaign performed flights in northern Canada and Alaska to monitor various properties during the change from winter to spring in the Arctic. The flights were made using the POLAR 5, a Basler BT-67 operated by the Alfred Wegener Institute for the study of the Arctic. PAMARCMiP aims to study meteorology, air quality and sea ice thickness.

A range of aerosol properties were measured, including aerosol number concentration, scattering and absorption coefficients, AOD, and black carbon concentration. The black carbon concentrations were measured with a single particle soot photometer. This instrument functions by drawing aerosol containing air into a chamber equipped with a 1060 nm laser and a set of detectors that detect in the visible range. The laser is shone onto the particles which scatter and absorb the light. The scattering allows calculation of the size of the particle, while the absorbed light causes the particles to heat up and eventually vaporize. As this heating occurs, the absorbing part of the particles emit light which is detected, the mass being determined by the intensity of the emitted light. The SP2 has a detection limit of 10 $\frac{ng}{m^3}$ (DMT, 2013), and the instrument agrees well with other black carbon measurement systems. A comparison with two other measurement systems found that mass measurements from all three instruments agreed to within 15% (Slowik et al., 2007). This system is ideal for an aircraft campaign as there are no filters to change, as well as a high time resolution.

A study of these black carbon measurements found that concentrations were decreasing aloft in comparison with previous airborne studies, in line with what was

being observed at various ground station monitoring sites (Stone et al., 2014). The aerosol property data has also proved useful for providing large scale pictures of the vertical structure of Arctic aerosol for comparison with models and satellite instruments (Stone et al., 2010). It has also been used for the study of individual events, such as a pollution event that occurred over Zeppelin mountain on Ny-Alesund, where the PAMARCMiP plane was able to collect data in conjunction with the station on the mountain, sampling the air mass out to a distance of 40 kilometers (Hoffman et al., 2012). This study provided an opportunity to see how parameters such as the size distribution of aerosols changed with height. Figure 3.2 shows the flight paths

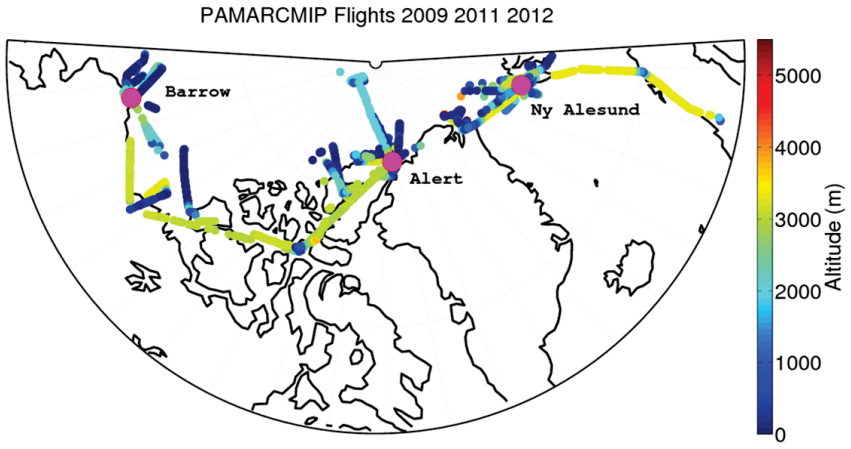

Figure 3.2: PAMARCMiP 2009, 2011 and 2012 flight tracks, along with in-situ ground monitoring stations.

taken by the plane. The flights took place between late March and early May of each year.

Chapter 4

Assessing the Implications of Emissions Types

This chapter interprets data from the measurements discussed in the previous chapter using different simulations in order to understand the implications of different emissions sources.

4.1 Models

The model used for these simulations is the GEOS-Chem global chemical transport model version 9.01.03. The model is driven by GEOS-5 meteorology provided by the NASA Global Modeling and Assimilation Office (Rienecker et al., 2008), with a 15 minute time step for transport and a 60 minute time step for chemistry and emissions. The grid size used was a 2° by 2.5° grid with 47 vertical levels up to 0.01 hPa. The model has a bulk aerosol mass simulation of sulphate and secondary organic aerosols (Park et al., 2004), sea salt (Jaeglé et al., 2011) , mineral dust (Farlie et al., 2010), and carbonaceous aerosols (Park et al., 2003). Organic carbon and black carbon are divided into hydrophilic and hydrophobic fractions. There is a fixed e folding time of 1.2 days for conversion from hydrophobic to hydrophilic (Chin et al., 2002). The hydrophilic aerosols are removed through in-cloud rainout, as well as the dry deposition and below cloud rainout that removes all aerosols (Bey et al., 2001).

All simulations were done with six months of spin up to ensure that starting conditions did not affect the model results. The emission inventories used for carbonaceous aerosol are the Bond inventory (Bond et al., 2007) that covers the entire world for a base year of 2000, and the Lu inventory (Lu et al., 2011) which covers India and

China for the years 1996-2010. These emissions were doubled in the regions of Russia and China following Wang et al. (2011) to account for increases in these emissions since 2000 due to the ongoing rapid growth of the Chinese economy which is coupled to increasing emissions, growing from 1200 Gg in 2000 to 1900 Gg in 2009 (Qin and Xie, 2012), as well as the rapid recovery of the Russian economy, which stagnated after the fall of communism (Aslund, 2007). Model states were output on a daily average basis, except for data that was collected coincidently with the PAMARCMiP flight campaign which output at points coinciding with measurements taken in the aircraft. Some simulations were modified by the addition of black carbon emissions from flaring and seasonal cycles for existing emissions as described in the next section.

GEOS-Chem has been previously used in the study of the arctic. One use was the identification of source regions for measurements taken during the ARCTAS flight campaign in 2008, as well as for measurements performed at several different monitoring stations (Wang et al., 2011). Another application of the model alongside data from various satellites to the Arctic region was to evaluate the impact of severe Russian wildfires in 2003 on the Arctic (Generoso et al., 2007). It has also been used for the study of compounds other than aerosols, for example one study used a version of GEOS-Chem coupled with an ocean model to study the sources of high levels of mercury found in the Arctic during the summer (Fisher et al., 2012).

4.2 Emissions Variations

In this work two main data sets are examined, the PAMARCMiP aircraft campaigns and ground level monitoring sites, as described in the second chapter. Four sets of simulations were performed. The first set used the standard GEOS-Chem emissions inventories for black carbon. The second set of simulations used the same total emissions as the first simulation, however seasonal variation was imposed on the emissions using the ECLIPSE (Evaluating the Climate and Air Quality Impacts of Short-lived

Pollutants) version 5 emissions inventory (Kilmont et al., 2013). The year used to calculate seasonal variation was 2010. The ECLIPSE inventory includes a representation of the seasonal variation in domestic heating. Annual total emissions from the base case simulation were scaled by monthly emissions from the ECLIPSE inventory.

The third set of simulations used the same emissions as the second set, however emissions from gas flaring were also added from the ECLIPSE inventory. This particular type of emission was chosen as it is one of the largest sources of black carbon emissions north of 60 degrees, along with the fact that the amount of flaring has risen in Northern Russia in recent years, increasing by an estimated 10 billion cubic meters between 1995 and 2006, displacing Nigeria as the world's largest source of gas flaring emissions (Elvidge et al., 2007).

The fourth set of simulations use the same emissions as the third set, however the emissions in various regions were set to zero in order to determine their total contribution to the pollution that is found in the Arctic. These regions were North America, Europe, Eastern Asia, and Northern Asia. A final simulation had no biomass burning emissions. Total global emissions, along with emissions above 65 degrees, are presented in figure 4.1. On a global scale, the residential and commercial sector is the largest emitter, however above 65 degrees the energy sector, which includes gas flaring, becomes dominant.

Figure 4.3 shows the average difference in black carbon concentrations between the simulations using the original Bond and Lu black carbon emissions inventories, whose concentrations are presented in figure 4.2, and the ones that use the Bond and Lu inventory with the seasonal cycle applied. These maps show a large difference in the winter months in Europe and north eastern China, whereas the difference is much smaller during the spring. This change is driven by the seasonal cycle of heating during the winter that was not represented adequately before by the original inventories. Figure 4.4 shows the difference in black carbon concentrations between the simula-

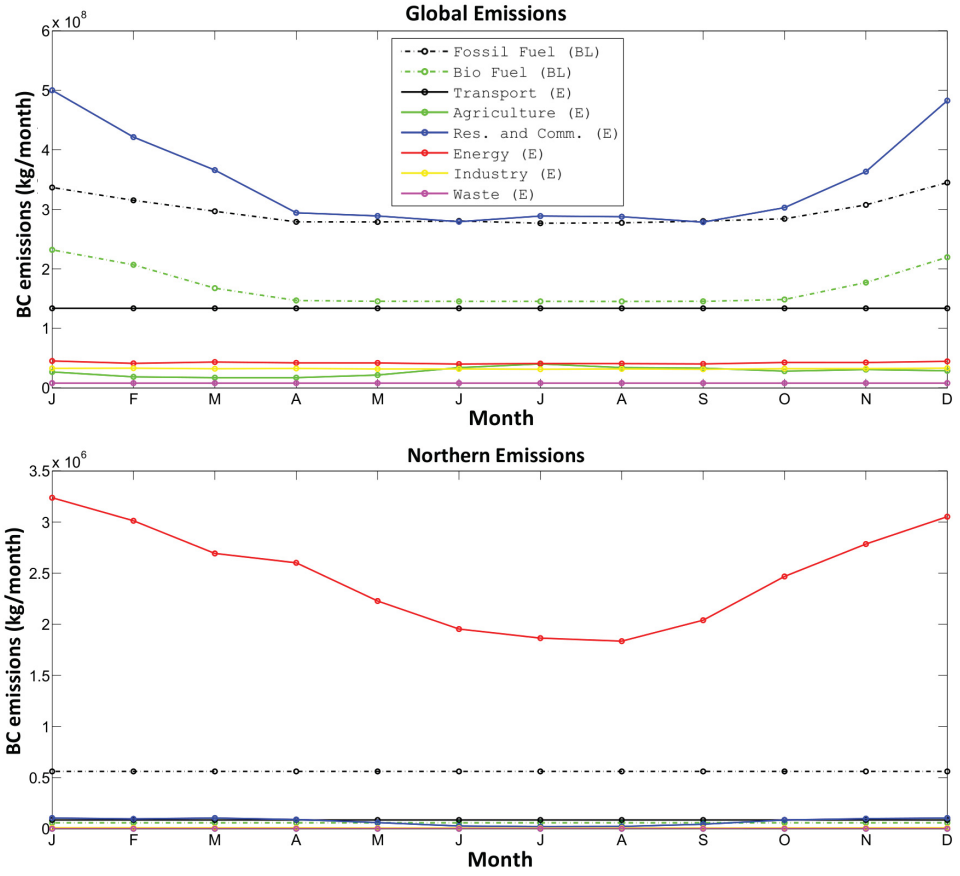

Figure 4.1: ECLIPSE and Bond/Lu emissions used in the simulations. Northern emissions are above 65 degrees latitude. Gas flaring emissions are included in the ECLIPSE energy line. E refers to ECLIPSE and BL refers to Bond/Lu. Res. and Comm. is Residential and Commercial.

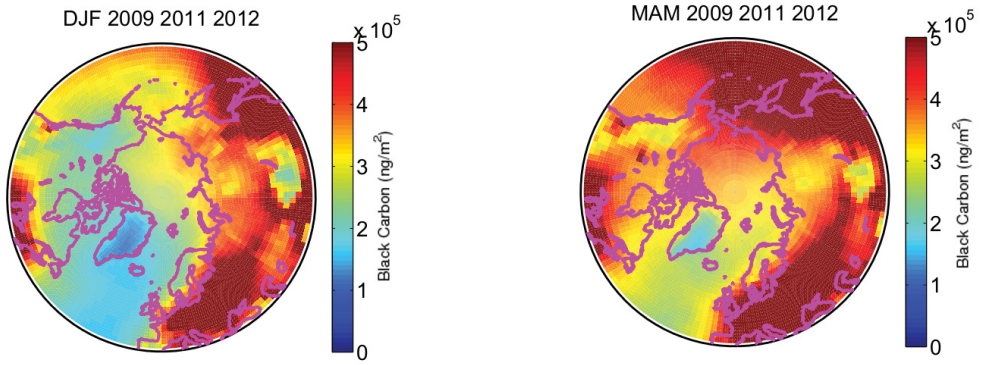

Figure 4.2: Column Arctic black carbon concentrations in the base GEOS-Chem simulation.

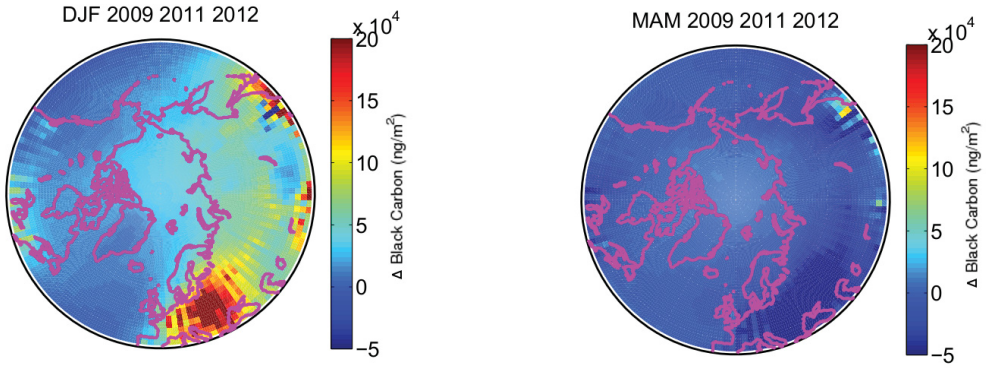

Figure 4.3: Black carbon concentration difference between simulations with seasonal cycle applied to emissions minus the original simulation with unchanged emissions. Negative values are due to the fact that emissions have shifted between months due to the applied seasonal cycle.

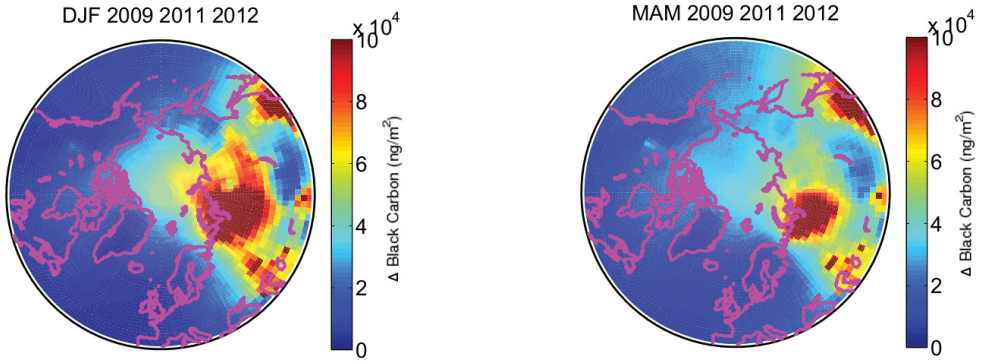

Figure 4.4: Black carbon concentration difference between simulation with original emissions minus the simulation with gas flaring emissions added to the original emissions.

tions using the original Bond and Lu inventories and the simulations with additional flaring from ECLIPSE added. There are large changes in northern Russia due to the additional gas flaring, along with north eastern China. This flaring appears to be higher during the winter than in the spring, due to a modest seasonal cycle above 65 degrees as seen in figure 4.1, as well as differences in transport during the winter and spring from flaring source regions.

4.3 Ground Level Sites

Several ground level sites were selected for analysis, detailed in chapter two. Not all of the sites had data that covered the same years as the simulations that were performed, and some had partial overlap.

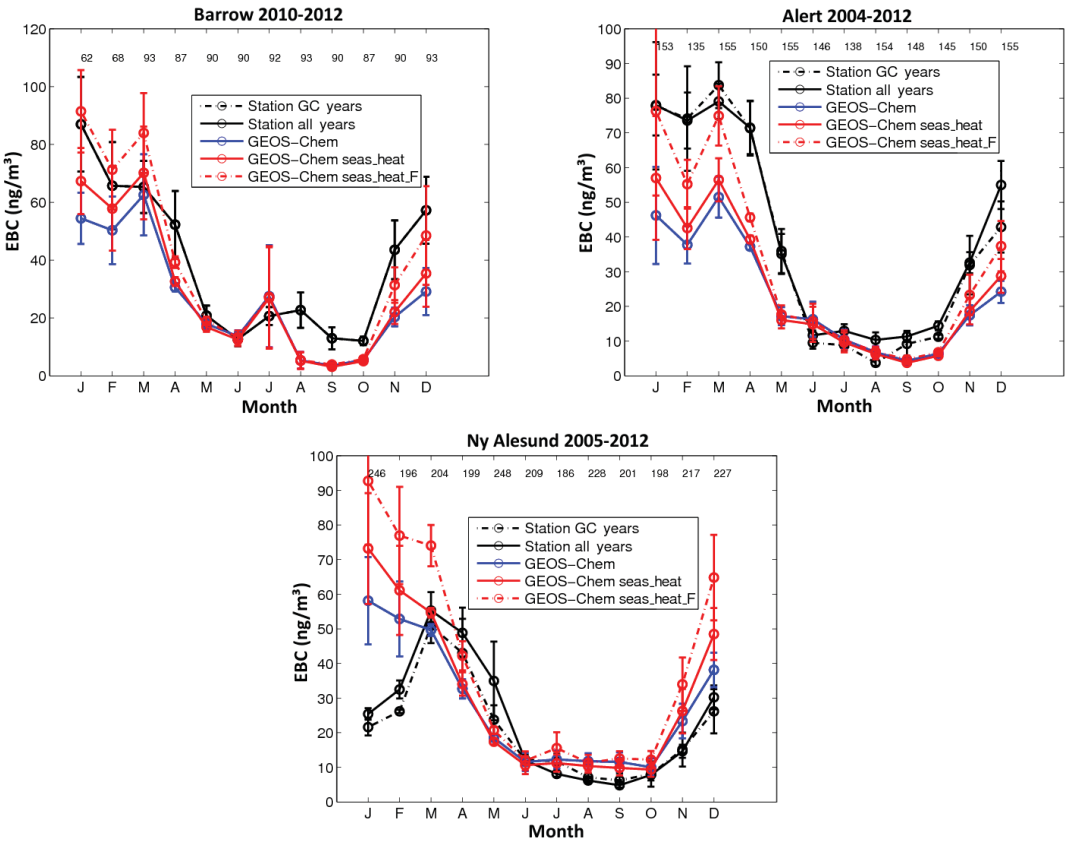

Figure 4.5: Ground level monitoring stations for black carbon concentrations. The line labeled Station all years are monthly averages that are calculated using all available points, while the lines labeled Station GC years are calculated from the years that overlap the simulation years, if any are available. The other lines refer to data from the original simulation (GEOS-Chem), the weighted simulation (GEOS-Chem seas heat) and the weighted simulation with additional flaring (GEOS-Chem seas heat F). Error bars are calculated from the standard deviation divided by the square root of the number of observations.

The comparisons against the first three sets of simulations are presented in figure 4.5. All sites show a seasonal cycle of black carbon concentration, however this cycle is not uniform across the entire Arctic. At Barrow there is a distinct peak in January,

whereas at Alert the concentrations stay roughly constant from January until April and then rapidly decrease. Ny-Alesund has quite a different cycle, peaking in March with lower concentrations through the winter months. In addition, the difference in magnitude between summer and winter concentrations varies as well, with a factor of 5 at Barrow, 6 at Ny-Alesund and 8 at Alert.

The original GEOS-Chem simulation partially represents the seasonal cycle of Arctic haze, however during the winter months there is a large underestimation at all sites with the exception of Ny-Alesund. Adjusting the original emissions with a seasonal cycle has a small effect on winter concentrations, however this change is insufficient to represent the observations. Looking at the difference between this simulation and the original simulation in figure 4.3, it appears that this change is mostly confined to Europe. The simulation that includes flaring in northern Russia does improve accuracy at Alert and Barrow in January, February and March, however the concentrations drop far too quickly during the transition from the high concentration levels during the Arctic haze period in the winter and early spring to the relatively clean periods during the summer. This transition, which occurs due to the increasing temperature as well as higher levels of moisture in the air, appears to be starting earlier in the model than what is seen from the in-situ measurements, particularly at Alert. This suggests issues with correctly modeling the removal processes during this changeover period.

Figure 4.6 examines the seasonal cycle at the Ny-Alesund site. Its location on top of a mountain at 474 meters is sometimes in the free troposphere which experiences different circulation. This is due to the fact that the height of the atmospheric boundary layer in the Arctic during the winter is quite shallow, with a height of around 100 meters during the winter in the vicinity of the station, rising to a maximum of around 550 meters during the winter (Zhang et al., 2011). This GEOS-Chem simulation does not reproduce this cycle in the grid box that contains the Ny-Alesund site four levels

above the surface, instead producing a cycle similar to what is seen at the other two sites. If the model is sampled in a grid box higher above this point, however, the cycle begins to show similarities to what is measured at the station at around 1.6 km which is 12 levels above the surface. Details of the GEOS-Chem grid can be seen in figure 4.17, as the points on the figure correspond to the vertical bins in GEOS-Chem.

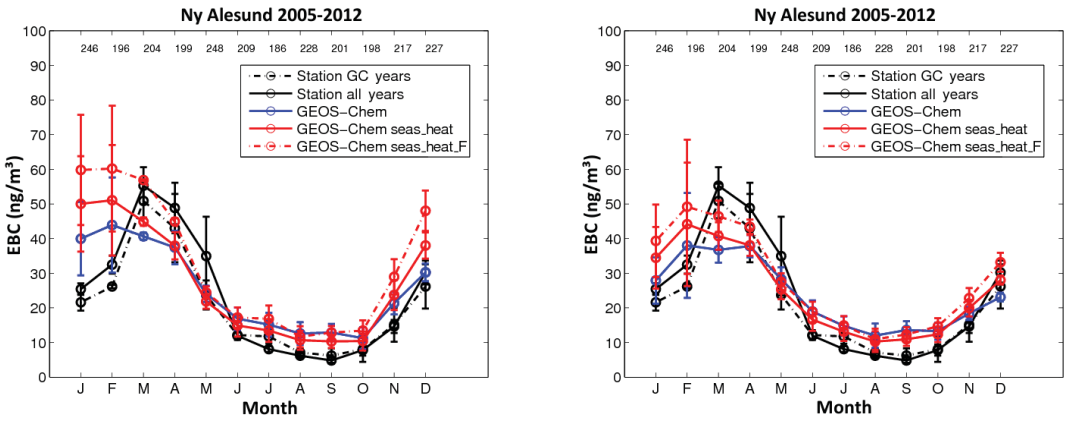

Figure 4.6: Black carbon at selected heights in the GEOS-Chem model above the Ny-Alesund station along with in-situ measurements. Simulation heights are 1 km on the left and 1.6 km on the right, station altitude is 474 m.

Figure 4.7 examines the day to day variation in black carbon concentrations. Measurements taken during the winter and early spring of 2012 at Alert indicate several instances of days with black carbon concentrations that are much larger than the surrounding values. The addition of a seasonal cycle along with additional flaring emissions has improved the ability of the model to represent these episodes, despite the fact that model emissions are constant throughout the month. The correlation between the two simulations and the in-situ measurements does not change very much, going from 0.70 to 0.72, however the slope greatly increases from 0.42 in the original simulation to 0.77 in the simulation that includes flaring emissions and a seasonal cycle, and the root mean squared error decreases from 49.16 $\frac{ng}{m^3}$ to 45.45 $\frac{ng}{m^3}$. Synoptic events contribute to episodic transport from source regions to the Arctic, for example a case study of an Arctic haze event in early March of 2007 detected by the

CALIPSO satellite found that the major factor for this episode was a cyclone that allowed for rapid vertical transport, along with a high pressure system in the north western pacific that facilitated rapid pole-wards transport (Di Pierro et al., 2011).

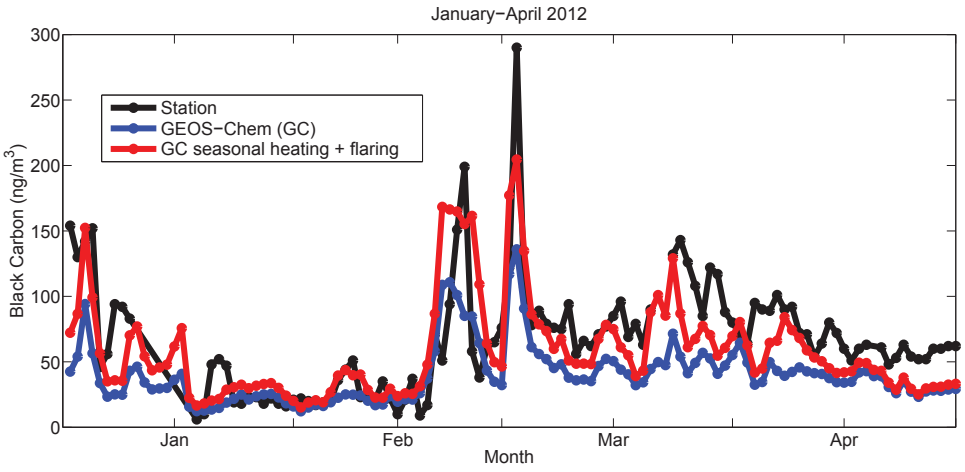

Figure 4.7: Comparison of Daily measurements at Alert along with daily simulation values.

Figure 4.8 shows carbon monoxide concentrations at the three sites. While there is good agreement with the measurements, even with the seasonal cycle applied and additional flaring emissions added there is an underestimate during the winter at all sites. Carbon monoxide is a useful chemical to examine in the study of black carbon as it is produced in the same processes as black carbon, however it is a gas, therefore it is not deposited out of the atmosphere like black carbon, which means that it can be used as a tracer for transport in the model (Pommier et al., 2010). In all cases, we see that the pattern does not change much from site to site, unlike black carbon at the Ny-Alesund site, which exhibits a much different cycle. This would suggest that this difference is rooted in the deposition scheme, as opposed to problems with transport, although the winter underestimation does indicate that the modeled transport processes are not perfect. This is reinforced by the accuracy shown in reproducing the daily measurements at Alert, which would depend strongly on proper transportation, as the emissions are not varied on a daily basis.

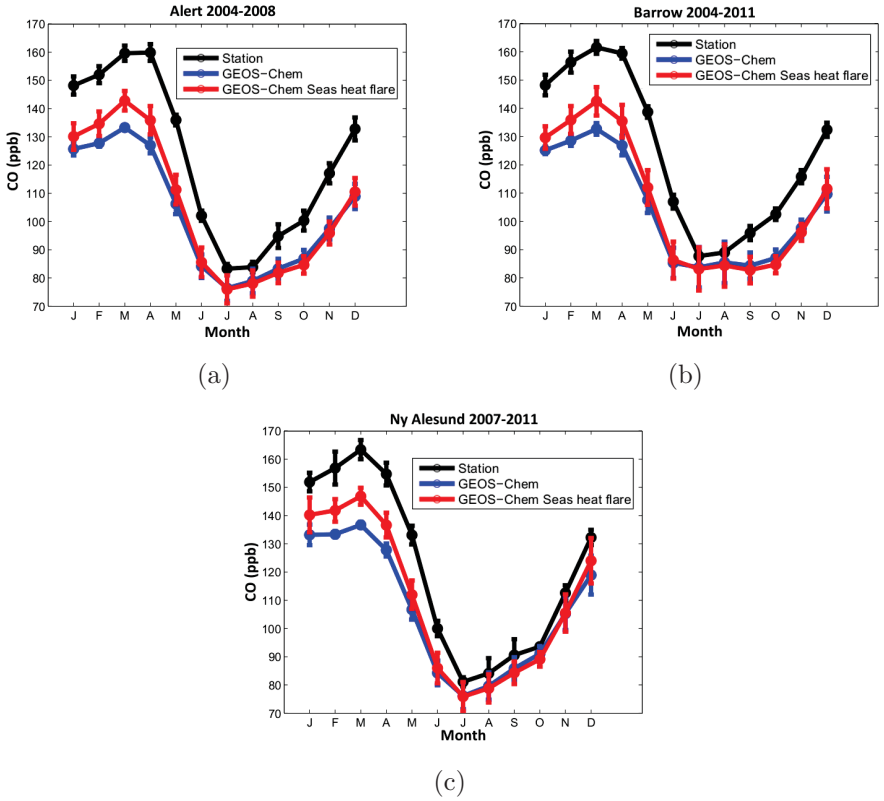

Figure 4.8: Ground level monitoring station comparisons for carbon monoxide, blue line is the original simulation while the red line is the simulation with a seasonal heating cycle applied, as well as additional flaring emissions.

4.4 Emissions Source Region Attribution

Sensitivity simulations were conducted to understand how different source regions affect Arctic black carbon. These regions are detailed in figure 4.9, with exact latitude and longitude ranges defined in table 4.1.

Region	Latitude Range	Longitude Range
North America	25N-90N	170W-50W
Europe	30N-90N	10W-60E
East Asia	10S-50N	60E-180E
North Asia	50N-90N	60E-180E

Table 4.1: Source region latitude and longitude ranges

Figure 4.10 shows the origins of black carbon at the three stations as predicted by the model. The major contributors to winter concentrations in the North American

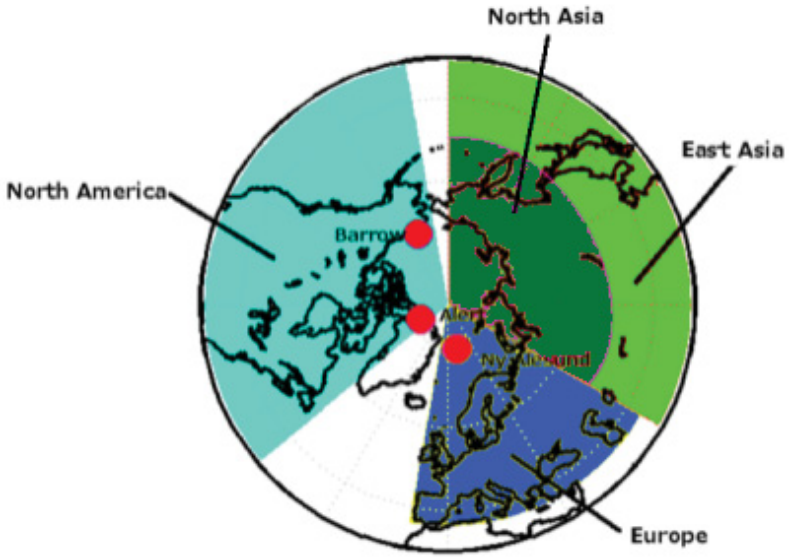

Figure 4.9: Source regions of simulated black carbon in GEOS-Chem. Colors correspond to following area plots.

Arctic are East Asia and Europe, with smaller contributions from Northern Asia and North America. The small size of the North American contribution is likely due to the fact that the majority of emissions in North America take place at lower latitudes than in other regions and the transport pathways to the Arctic are not as direct. During the summer, biomass burning emissions begin to play a larger role as human activity and dry vegetation mix to create wildfires. At the Ny-Alesund site, a similar distribution is seen, except that Europe plays a much more prominent role.

These findings are consistent with other research on the origins of Arctic pollution. One study which analyzed the same three sites using the FLEXPART model to calculate back trajectories found that air parcels arriving from Northern Eurasia (Europe and parts of Northern and Eastern Asia) were associated with high concentrations of black carbon, whereas those arriving from North America were lower (Hirdman et al., 2010). A similar study which examined both Alert and Barrow found that at Alert the main source regions were Siberia and Europe, whereas at Barrow the main source

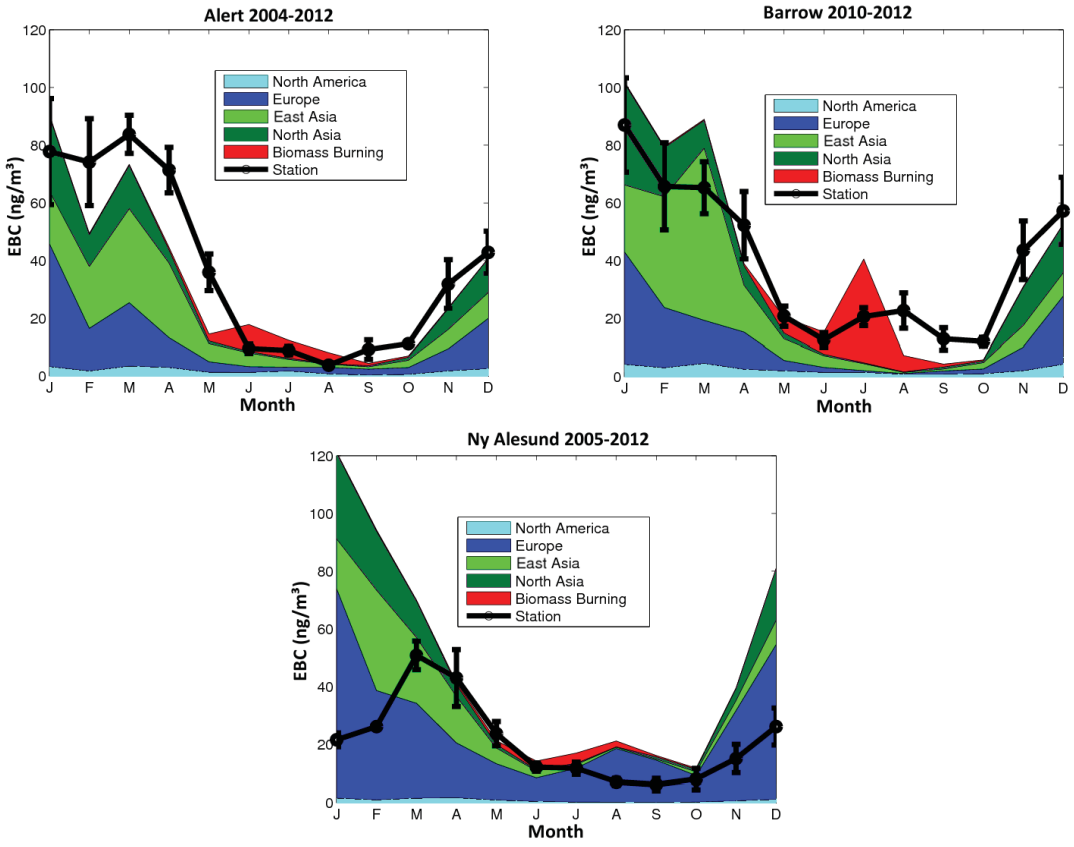

Figure 4.10: Monthly averages of black carbon at selected Arctic measurement sites color coded to the origin of the emissions.

regions were Siberia and Asia (Sharma et al., 2006). A third study which focused on the Arctic region as a whole, but used a similar approach by doing a sensitivity study using the ECHAM5-HAMMOZ found similar contributions from Siberia, Asia and Europe, with smaller contributions from North America (Bourgeois and Bey, 2011).

In addition to examining single sites, it is also interesting to examine the entire area of the Arctic, as well as the vertical changes in black carbon concentrations. Figure 4.11 presents seasonal concentrations of black carbon in the Arctic, averaged over the region from 70 to 90 degrees North, and 180 degrees East to 180 degrees West. During the winter there are highly elevated levels of black carbon near the ground, which are seen in the ground station comparison section. These concentrations, however, decrease rapidly with increasing altitude, until levels are comparable

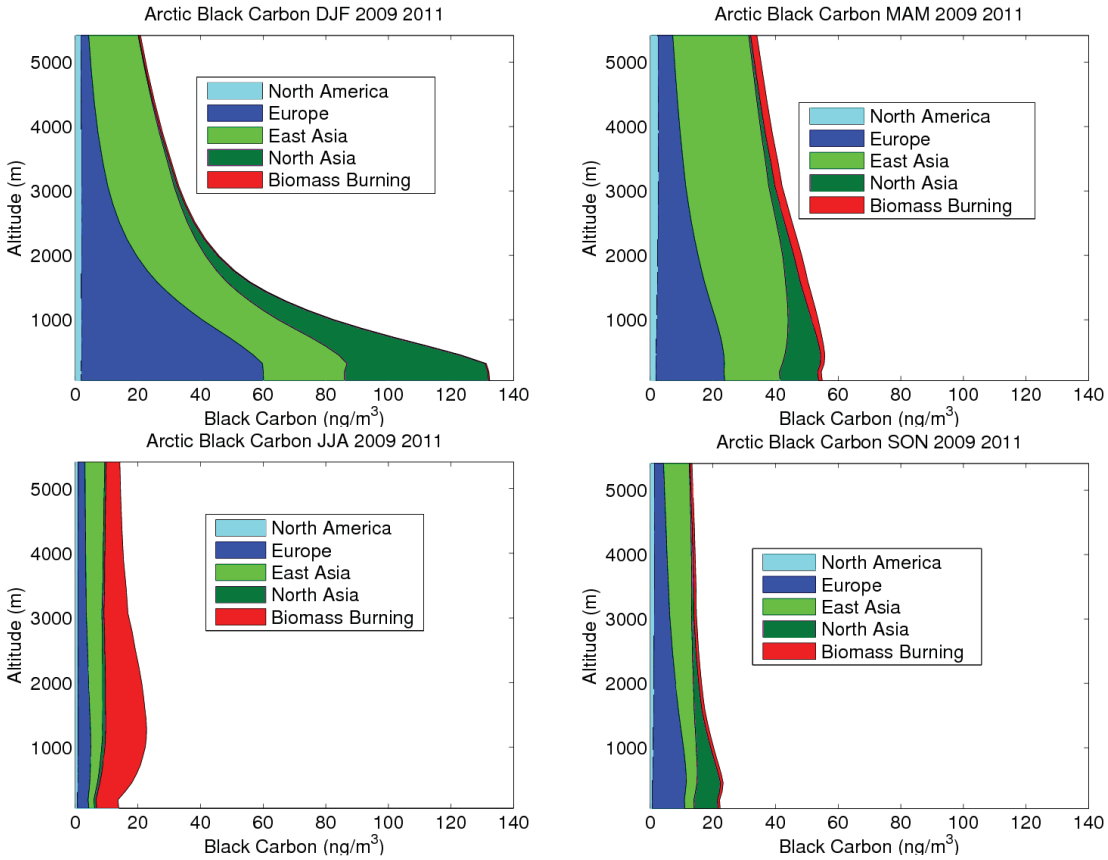

Figure 4.11: Vertical profiles of black carbon in the arctic averaged seasonally. The area defined as the arctic for these figures is from 70 degrees north to 90 degrees north, over all longitudes. Concentration amounts are color coded to their emission source regions.

to other seasons at higher altitudes. During the winter, spring, and fall, upper altitude concentrations are dominated by East Asian emissions while during the summer biomass burning tends to dominate. This is due to the fact that air masses originating from East Asia sometimes experience rapid vertical transport due to local weather conditions such as being lifted by mid-latitude cyclones (Di Pierro et al., 2011), as well as being forced upwards by the low potential temperature surfaces at the surface in the arctic during the winter, as air originating from East Asia is warm and moist, and cannot pass through these surfaces (Stohl, 2006). During summer, the dominant contributor to black carbon mass both aloft and near the ground is biomass burning. While there are wildfires that are started by natural causes such as lightning, it

has been estimated that between 85-90 % of wildfires are caused by human activity, accounting for 50-60% of the total burned area, with climate change expected to increase to both the number and size of these fires (Christensen et al., 2013). Above 2000 meters, there is some variation in concentration, going from around 20 $\frac{ng}{m^3}$ in the summer, to around 50 $\frac{ng}{m^3}$ in the winter. Below 2000 meters, especially near the surface, there is a dramatic change, from below 20 $\frac{ng}{m^3}$ in the summer to around 130 $\frac{ng}{m^3}$ in the winter. These differences show that the winter Arctic haze phenomenon is mainly contained in the lower atmosphere, trapped in the polar dome, which is the name given to the cold, stable air near the surface in the Arctic. The dome can extend as far south as 40 degrees in parts of Europe and Asia, making these the dominant source regions of the Haze (Law and Stohl, 2007). In the lower troposphere, Europe and Northern Asia become important sources in the winter, spring, and fall, although East Asia still contributes a significant amount. During the summer, biomass burning emissions dominate at all altitudes. Similar to the surface source region comparisons, these results are consistent with what others have found. A comparison of 17 different models found that Europe tended to dominate concentrations low in the atmosphere, and become less important with altitude, whereas East Asia became more important with altitude, and North America remained roughly constant (Shindell et al., 2008). Another sensitivity study performed using the Global Environmental Multiscale model with Air Quality processes (GEM-AQ) model found that Europe and Northern Asia were the largest source regions near the surface, decreasing with altitude, with East Asia and North America becoming larger with altitude (Huang et al., 2010).

4.5 PAMARCMiP

The PAMARCMiP campaign has currently collected data in 2009, 2011, and 2012. Figure 4.12 shows the location and altitude of each data point collected during the

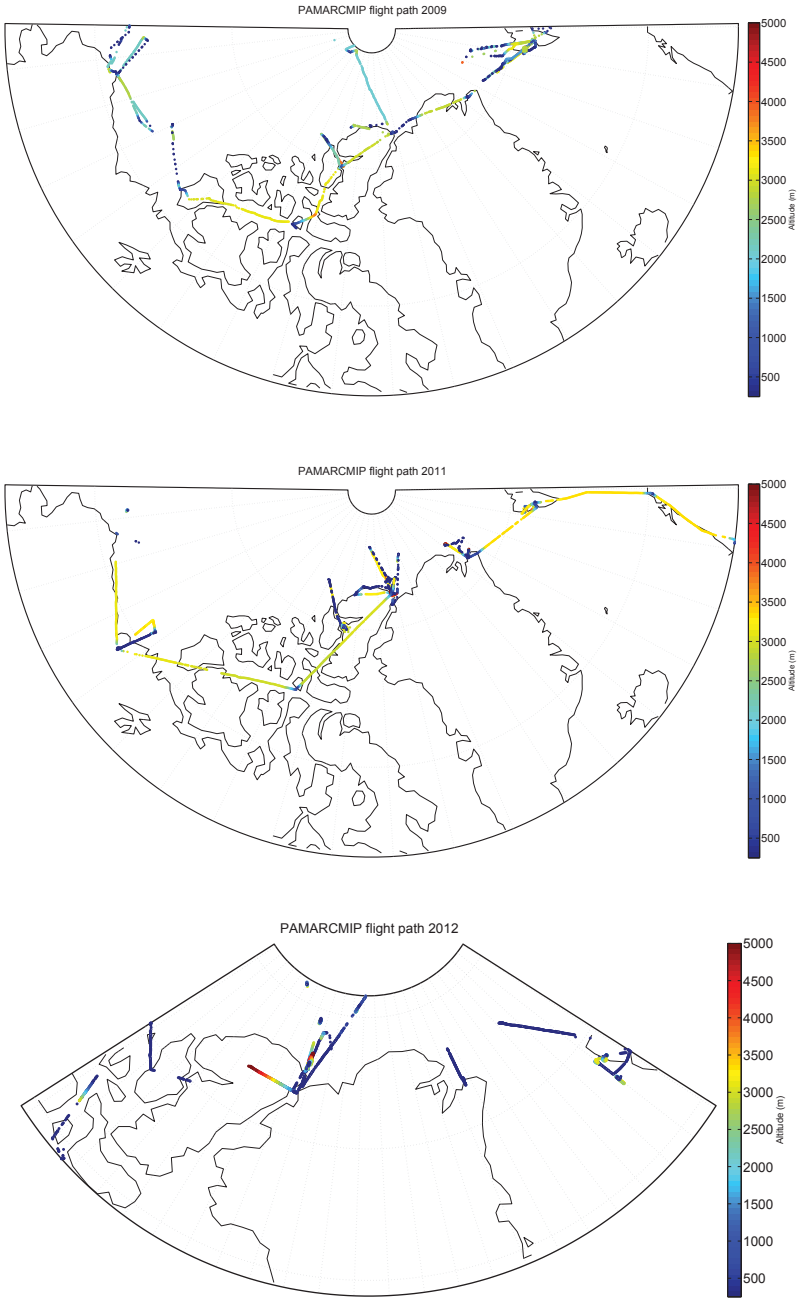

Figure 4.12: PAMARCMiP flight tracks 2009, 2011, and 2012. Dots represent points where usable data was collected.

PAMARCMiP campaign. During each simulation, values were archived for each of these points at the nearest grid box and time step.

Alert in northern Canada presents a unique opportunity as there are a variety of

instruments located at the research station there, as well as the fact that the PAMARCMiP campaign performed flights around the area. A comparison of PAMARCMiP measurements with other instruments is necessary due to the fact that there were differences in the concentrations measured by the SP2 from year to year, as well as different SP2 instruments in use. Figure 4.13 presents airborne measurements taken

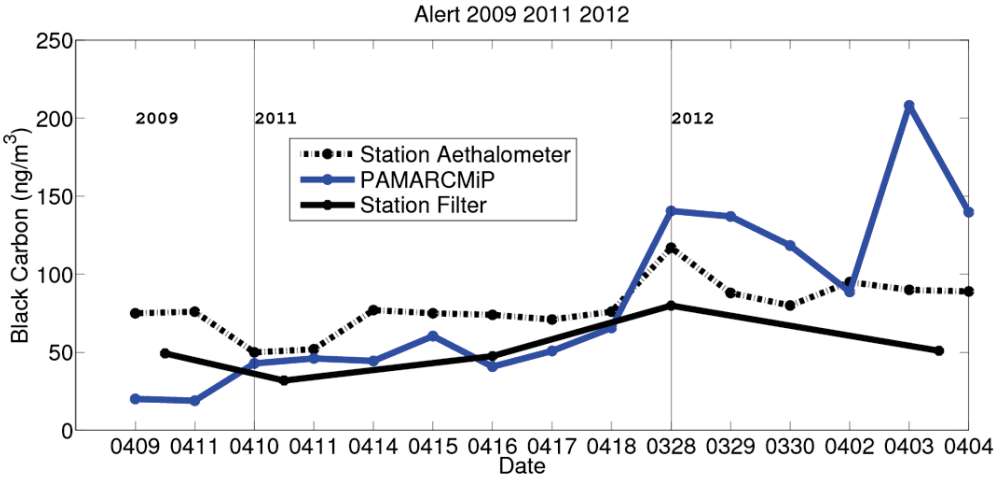

Figure 4.13: Measurements of black carbon around Alert using Aethalometer, weekly filter, and SP2.

during the PAMARCMiP campaign in the vicinity of Alert (within 2 degrees of latitude and 12 degrees of longitude) up to a maximum altitude of 1000 meters, along with ground level measurements from Alert Station. In 2009 and 2011 aircraft and ground measurements agree to within an average of 24 $\frac{ng}{m^3}$. It is puzzling that the concentrations measured by PAMARCMiP are so much higher in 2012 than in the other two years, a phenomenon that is not reflected in the ground level measurements with average difference increasing to 63.5 $\frac{ng}{m^3}$. This is seen at the Ny-Alesund site as well, in figure 4.14, thus we focus the rest of our analysis on 2009 and 2011. Over 2009 and 2011, the modeled values both on the ground as well as coincidently sampled along flight paths had excellent agreement, with average agreements of 17 $\frac{ng}{m^3}$ on the ground, and 21 $\frac{ng}{m^3}$ in the air.

Figure 4.15 shows the PAMARCMiP data gridded onto the GEOS-Chem grid,

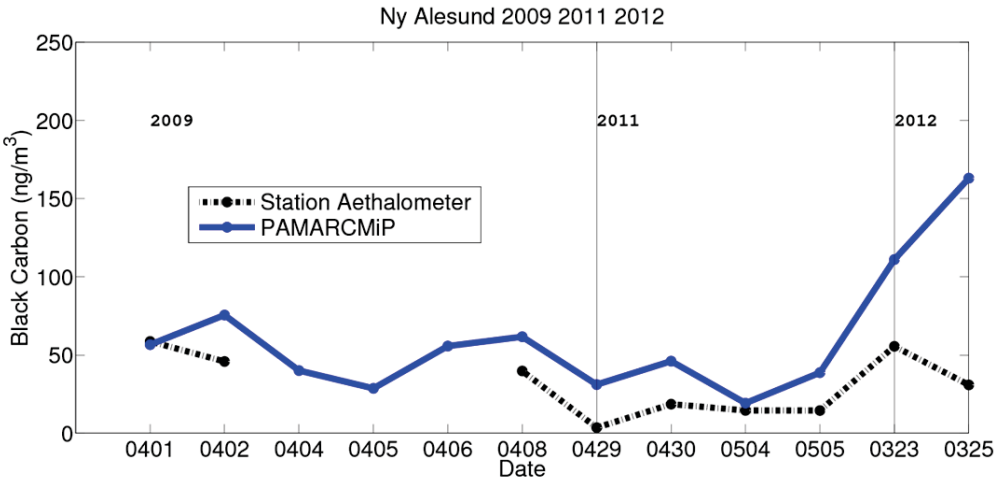

Figure 4.14: Measurements of black carbon around Ny-Alesund using Aethalometer and SP2.

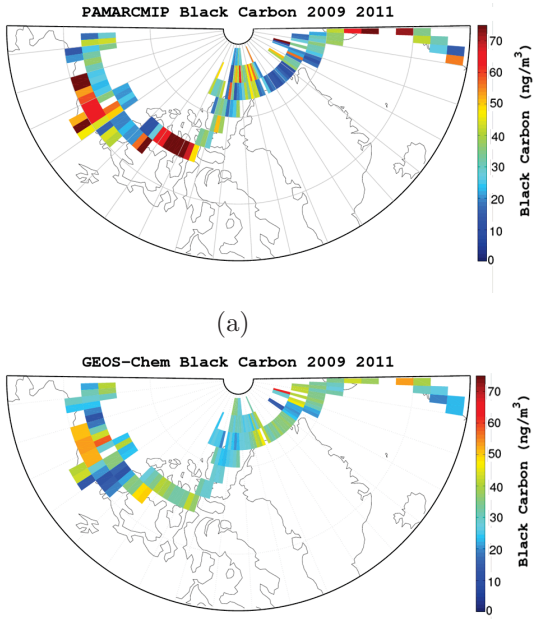

(a)

(b)

Figure 4.15: A is PAMARCMiP black carbon concentrations on the GEOS-Chem grid, b is coincidently sampled points from the simulation on the GEOS-Chem grid. Concentrations are averaged from the points in a given bin, and all data is included (April 3rd-25th 2009, March 30th-May 5th 2011).

along with modeled concentrations. In general, we see that the addition of flaring does not completely resolve the individual points of high concentration in the PAMARCMiP data, however most general areas of high concentration are matched in

2009 and 2011. Also, in general concentrations in the west are higher than what was measured in the east.

Sensitivity simulations were conducted to identify the sources contributing to the observed black carbon. Figure 4.16 shows the contribution of each source region to the simulated black carbon at each level. At all levels, emissions from East Asia dominate, therefore the high western concentrations are likely due to plumes from this region, with lower concentrations in the east originating from Europe. Biomass burning emissions are negligible at all levels, and North America makes a modest contribution. Each grid box does not represent a full vertical column, therefore it is necessary to examine the data on the vertical GEOS-Chem grid as well.

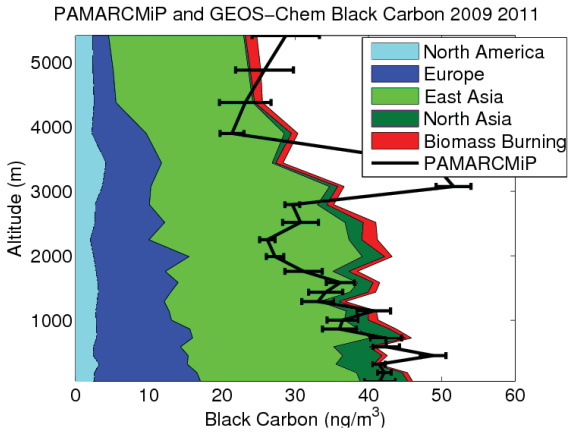

Figure 4.16: Vertical profile of black carbon in the Arctic from points taken coincidently with PAMARCMiP data, color coded to source region. The time-frame of this data is late March until late April of 2009 and 2011.

Figure 4.17 shows comparisons of vertical profiles made from these measurements, along with modified GEOS-Chem simulations. We see that the addition of gas flaring and a seasonal cycle shows good agreement with the measurements in the lower part of the atmosphere up to about 1500 meters. Above this point there is an overestimation until around 3000 meters where there is a large rise in concentration to a level higher than what is measured near the ground. This large rise is likely a concentrated plume

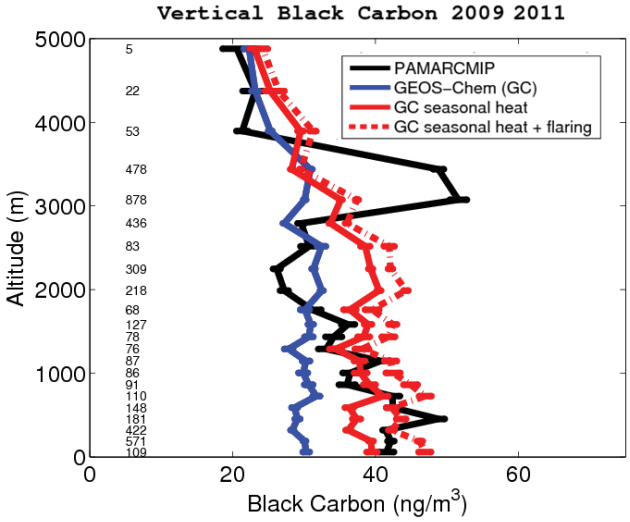

Figure 4.17: Vertical black carbon profile of PAMARCMiP and simulation data. Numbers refer to the number of data points in each box.

that was not represented in the model. A possible source may be biomass burning as April 2009 had an above average number of wildfires, with 31% more fires and 38% more total acreage burned than the average amounts in the previous ten years in the United States (NOAA, 2009). It should be noted that these profiles only represent a small portion of time and space in the Arctic, and that some levels contain a higher number of points than others. There is unfortunately no continuous record of high altitude black carbon measurements, only brief snapshots. One important fact is that these measurements are much lower than the ones that were collected during the AGASP campaigns of 1983 and 1986. For example, the second AGASP campaign which was conducted during the same part of the year as PAMARCMiP, found concentrations of around 300-500 $\frac{ng}{m^3}$ in the lower atmosphere, decreasing to concentrations of 25-100 $\frac{ng}{m^3}$ at an altitude of around 8 km (Hansen and Novakov, 1989).

Chapter 5

Conclusions

Black carbon concentrations from three Arctic measurement sites, Alert, Barrow, and Ny-Alesund, along with measurements taken during the PAMARCMiP flight campaign, were interpreted with the GEOS-Chem chemical transport model. The Arctic sites performed measurements using an Aethalometer, whereas the flight campaign measurements were performed with a Single Particle Soot Photometer (SP2). Concentrations measured by the Aethalometer are generally higher than those measured by the SP2 due to the fact that the Aethalometer is unable to distinguish between black carbon and other absorbing compounds, and the SP2 measures a limited range of particle sizes. In order to examine the seasonal cycle of Arctic black carbon, model emissions were modified in a couple ways. A seasonal cycle derived from the ECLIPSE inventory was applied to the original anthropogenic black carbon emissions. The main contributor to this cycle was domestic heating which peaked in the winter. The second modification that was performed was the addition of gas flaring emissions to the original emissions. As well as simulations involving global emissions modifications, a series of simulations were performed without emissions in several regions in the northern hemisphere, as well as one with no biomass burning emissions. These were performed in order to determine the amount of pollution each region was contributing to the total amount of pollution that is measured in the Arctic. These regions were North America, Europe, North Asia, and East Asia.

Long term comparisons at the Alert and Barrow sites found that simulations that

included both the seasonal cycle and the additional flaring emissions matched the in-situ measurements quite well during the winter, with the average difference between the simulation and the measurements in December, January, and February improving from 28.9 $\frac{ng}{m^3}$ to 8.6 $\frac{ng}{m^3}$ at Alert and from 25.5 $\frac{ng}{m^3}$ to 6.3 $\frac{ng}{m^3}$ at Barrow. This indicates that flaring emissions are quite an important contributor to wintertime Arctic black carbon concentrations as the original emissions inventory did not include these emissions. The seasonal cycle did improve agreement, however it was not as important a contribution as the flaring emissions, improving agreement to 22.2 $\frac{ng}{m^3}$ at Alert and to 16.5 at $\frac{ng}{m^3}$ at Barrow.

In addition to long term average comparisons, daily values were considered as well at the Alert site. The addition of flaring emissions improved the simulated concentrations of days with high concentration events. In addition to illustrating the impact that flaring emissions are having in the Arctic, as the Alert site is located at quite a distance from the origin of the emissions, this indicates that the modeled transportation pathways have some skill, as the model emissions are varied on a monthly basis. This is supported by comparisons of simulated and measured carbon monoxide concentrations at Alert with an annual average monthly difference of 15.4 ppb, as carbon monoxide is a tracer for transport.

The comparison of different measurement methods in the vicinity of the Alert and Ny-Alesund stations, along with comparisons of the PAMARCMiP campaign highlight some difficulties in recreating the transition period from a relatively polluted Arctic in the winter and spring to a more pristine environment in the summer. In general there was reasonable agreement between the simulation and measurements at most altitudes except for one area which was suspected to be a biomass burning plume that was not reproduced in the simulation. The improvements in agreement from the various modifications were confined to the lower part of the atmosphere

below around 1500 meters. Also the addition of flaring emissions did not improve the simulation at all altitudes, as sometimes the simulation with only the seasonal heating cycle applied was closer to the measured concentration, while at other altitudes the simulation with both was more accurate. The difference in concentrations between the the base simulation and the simulation with all modifications decreased with altitude from 16.1 $\frac{ng}{m^3}$ at the surface until the simulations converge above 3000 meters, and again at 5000 meters. While it is difficult to determine whether the additional flaring emissions are as important during this time period as during the winter months, there is evidence that the domestic seasonal heating cycle is quite important during this time period, at least in the lower parts of the atmosphere.

From the study of the contributions of different source regions to Arctic black carbon concentrations, we can draw a number of conclusions. Transport from East Asia is dominant aloft during the winter, spring, and fall above an altitude of roughly 2000 meters. In the lower troposphere, Europe and Northern Asia become important sources in the winter, spring, and fall, although East Asia still contributes a significant amount. During the summer, biomass burning emissions dominate at all altitudes.

This work has shown the importance of both the seasonal heating cycle of residential burning emissions as well as flaring emissions to concentrations of black carbon in the Arctic, especially during the winter. Some next steps that are worth exploring are evaluating these modifications with in-situ measurements both on the ground and aloft in other parts of the world. This would lend insight into which other regions are being affected by the practice of gas flaring, and the importance of these changes in other parts of the world. Another area that would be of interest would be further analysis of the period of change in March, April and May from polluted to pristine conditions, due to the difficulty in modelling this time period in the Arctic. Coordination with a flight campaign would be ideal, with many vertical profiles in the lower

portion of the atmosphere, as this area seems to be the part that is most affected by the changes explored in this work. In addition, these modifications should be evaluated alongside any improvements to the aerosol scavenging routines in the model to see if scavenging changes alone can improve the simulation of the March to May transitional period, or if emissions modifications have a role to play as well. Also, a more sophisticated approach to applying a seasonal cycle to the existing emissions would be required for a mature version of these changes if they were to be included in the standard GEOS-Chem model. This would require determining the biofuel and fossil fuel portions of each of the different sectors in the ECLIPSE inventory, from which the seasonal cycle used in this work is derived.

Bibliography

Aslund, A. (2007). *How capitalism was built: the transformation of Central and Eastern Europe, Russia, the Caucasus, and Central Asia*. Cambridge University Press.

Bey, I., Jacob, D., Logan, J., and Yantosca, R. (2001). Asian chemical outflow to the pacific in spring: Origins, pathways and budgets. *Journal of Geophysical Research*, 106:23097–23113.

Bodhaine, B. (1995). Aerosol absorption measurements at barrow, mauna loa and the south pole. *Journal of GeophysicalRresearch*, 100:8967–8975.

Bond, T., Bhardwaj, E., Dong, R., Jogani, R., Jung, S., Roden, C., Streets, D., and Trautmann, N. (2007). Historical emissions of black and organic carbon aerosol from energy related combustion, 1850-2000. *Global Biogeochemical Cycles*, 21:GB2018.

Bond, T., Doherty, S., Fahey, D., Forster, P., Berntsen, T., DeAngelo, B., Flanner, M., Ghan, S., Karcher, B., Koch, D., Kinne, S., Kondo, Y., Quinn, P., Sarofim, M., Schultz, M., Venkataraman, C., Zhang, H., Zhang, S., Bellouin, N., Guttikunda, S., Hopke, P., Jacobson, M., Kaiser, J., Kilmont, Z., Lohmann, U., Schwartz, J., Shindell, D., Storelvmo, T., Warren, S., and Zender, C. (2013). Bounding the role of black carbon in the climate system: a scientific assessment. *Journal of Geophysical Research*, 118:5380–5552.

Bourgeois, Q. and Bey, I. (2011). Pollution transport efficiency toward the arctic: Sensitivity to aerosol scavenging and source regions. *Journal of Geophysical Research*, 116:D08213.

Cao, J., Lee, S., Chow, J., Watson, J., Ho, K., Zhang, R., Jin, Z., Shen, Z., Chen, G., Kang, Y., Zou, S., Zhang, L., Qi, S., Dai, M., Cheng, Y., and Hu, K. (2007). Spatial and seasonal distributions of carbonaceous aerosols over china. *Journal of Geophysical Research: Atmospheres*, 112:D22S11.

Carrivain, O. and Orain, M. (2013). Two-photon laser-induced fluorescence for detection of carbon monoxide in aircraft combustion chamber. 13th ONERA-DLR Aerospace Symposium, Palaiseau, May 27th to 29th, 2013.

Cess, R. (1983). Arctic aerosol model estimates of interactive influences upon the surface-atmosphere clear sky radiation budget. *Atmospheric Environment*, 17:2555–2564.

Charlson, R., Schwartz, K., Hales, J., Cess, R., Coakley, J., Hansen, J., and Hoffman, D. (1992). Climate forcing by anthropogenic aerosols. *Science*, 255:423–429.

Chen, Y., Zhi, G., Feng, Y., Zhang, G., Li, J., Sheng, G., and Fu, J. (2009). Measurements of black and organic carbon emission factors for household coal combustion in china: implication for emission reduction. *Environmental Science Technology*, 43:9495–9500.

Chin, M., Ginoux, P., Kinne, S., Torres, O., Holben, B., Duncan, B., Martin, R., Logan, J., Higurashi, A., and Nakajima, T. (2002). Tropospheric aerosol optical thickness from the gocart model and comparisons with satellite and sunphotometer measurements. *Journal of Atmospheric Science*, 59:461–483.

Christensen, J., Hamilton, B., Glennon, R., Hoekstra, J., Male, T., Swetnam, T., Tobin, M., Day, M., Elliot, M., Levine, M., Ott, C., and weldon, S. (2013). Region at risk: Visualizing environmental trends in the american west. Report.

Clarke, A. and Noone, K. (1985). Soot in arctic snowpack: A cause for perturbation in radiative transfer. *Atmospheric Environment*, 19:2045–2053.

Di Pierro, M., Jaeglé, L., and Anderson, T. (2011). Satellite observations of aerosol transport from east asia to the arctic: three case studies. *Atmospheric Chemistry and Physics*, 11:2225–2243.

DMT (2013). Sp2: Single particle soot photometer. Brochure.

EC (2010). Canadian climate normals 19812010. `ftp://ftp.tor.ec.gc.ca/Pub/Normals/English/English_CSV_files/NU/NU_ALER-WHAL_ENG.csv`. Accessed: 2015-01-09.

EIA (2014). Monthly energy review: November 2014. Report.

Eleftheriadis, K., Vratolis, S., and Nyeki, S. (2009). Aerosol black carbon in the european arctic: Measurements at zeppelin station, ny-alesund, svalbard from 1998-2007. *Geophysical Research Letters*, 36:L02809.

Elvidge, C., Baugh, K., Tuttle, B., Howard, A., Pack, D., Milesi, C., and Erwin, E. (2007). *A Twelve Year Record of National and Global Gas Flaring Volumes Estimated Using Satellite Data*. World Bank.

ESRL, N. (2014). Measuring and analyzing greenhouse gasses. `http://www.esrl.noaa.gov/gmd/ccgg/behind_the_scenes/meas_analyzers.html`. Accessed: 2014-05-14.

Farlie, T., Jacob, D., Dibb, J., Alexander, B., Avery, M., van Donkelaar, A., and Zhang, L. (2010). Impact of mineral dust on nitrate, sulfate, and ozone in transpacific asian pollution plumes. *Atmospheric Chemistry and Physics*, 10:3999–4012.

Fisher, J., Jacob, D., Soerensen, A., Amos, H., Steffen, A., and Sunderland, E. (2012). Riverine source of arctic ocean mercury inferred from atmospheric observations. *Nature Geoscience*, 5:499–504.

Generoso, S., Bey, I., Attié, J., and Bréton, F. (2007). A satellite and model based assessment of the 2003 russian fires: Impact on the arctic region. *Journal of Geophysical Research*, 112:D15302.

Hansen, A. (2005). *The Aethalometer*. Magee Scientific.

Hansen, A. and Novakov, T. (1989). Aerosol black carbon measurements in the arctic haze during agasp 2. *Journal of Atmospheric Chemistry*, 9:347–361.

Hansen, A., Rosen, H., and Novakov, T. (1984). The aethalometer: an instrument for real time measurement of optical absorption by aerosol particles. *The Science of the Total Environment*, 36:191–196.

Hegg, D., Livinston, P., Hobbs, P., Novakov, T., and Russel, P. (1997). Chemical apportionmentof aerosol column optical depth off the mid-atlantic coast of the united states. *Journal of Geophysical Research*, 102:25293–25303.

Heintzenburg, J. (1988). Fine particles in the global troposphere: A review. *Tellus*, 41B:149–160.

Herber, A., Thomason, L., Gernandt, H., Leiterer, U., Nagel, D., Schulz, K., Kaptur, J., Albrecht, T., and Notholt, J. (2002). Continuous day and night aerosol optical depth observations in the arctic between 1991 and 1999. *Journal of Geophysical research*, 107:4097.

Hirdman, D., Burkhart, J., Sodemann, H., Eckhardt, S., Jefferson, A., Quinn, P., Sharma, S., Strom, J., and Stohl, A. (2010). Long term trends of black carbon and sulphate aerosol in the arctic: changes in atmospheric transport and source region emissions. *Atmospheric Chemistry and Physics*, 10:9351–9368.

Hoffman, A., Osterloh, L., Stone, R., Lampert, A., Ritter, C., Stock, M., Tunved, P., Hennig, T., Böckmann, C., Li, S., Eleftheriadis, K., Maturilli, M., Orgis, T., Herber, A., Neuber, R., and Dethloff, K. (2012). Remote sensing and in-situ measurements of tropospheric aerosol, a pamarcmip case study. *Atmospheric Environment*, 52:56–66.

Huang, L., Gong, S., Jia, C., and Lavou, D. (2010). Relative contributions of anthropogenic emissions to black carbon aerosol in the arctic. *Journal of Geophysical Research: Atmospheres*, 115:D19208.

IPCC (2013a). *Climate Change 2013: The Physical Science Basis. Contribution of Working Group I to the Fifth Assessment Report of the Intergovernmental Panel on Climate Change*, page 1064. Cambridge University Press.

IPCC (2013b). *Climate Change 2013: The Physical Science Basis. Contribution of Working Group I to the Fifth Assessment Report of the Intergovernmental Panel on Climate Change*, page 694. Cambridge University Press.

IPCC (2013c). *Climate Change 2013: The Physical Science Basis. Contribution of Working Group I to the Fifth Assessment Report of the Intergovernmental Panel on Climate Change*, page 683. Cambridge University Press.

Jacob, D. (1999). *Introduction to Atmospheric Chemistry*, pages 144–146. Princeton University Press.

Jaeglé, L., Quinn, P., Bates, T., Alexander, B., and Lin, J. (2011). Global distribution of sea salt aerosols: New constraints from in situ and remote sensing observations. *Atmospheric Chemistry and Physics*, 11:3137–3157.

Kaskaoutis, D., Kambezidis, H., Hatzianastassiou, N., Kosmopoulos, P., and Badarinath, K. (2007). Aerosol climatology: dependence of the angstrom exponent on wavelength over four aeronet sites. *Atmospheric Chemistry and Physics Disscussions*, 7:7347–7397.

Kilmont, Z., Kupiainen, K., Heyes, C., Cofala, J., Rafaj, P., Höglund-Isaksson, L., Borken, J., Schöpp, W., Winiwarter, W., Purohit, P., Bertok, I., and Sander, R. (2013). *ECLIPSE V4a: Global emission data set developed with the GAINS model for the period 2005 to 2050*. International Institute for Applied Systems Analysis.

Lack, D., Moosmüller, H., McMeeking, G., Chakrabarty, R., and Baumgardner, D. (2013). Characterizing elemental, equivalent black and refractory black carbon aerosol particles: a review of techniques, their limitations and uncertainties. *Analytical and Bioanalytical Chemistry*, 406:99–122.

Law, K. and Stohl, A. (2007). Arctic air pollution: Origins and impacts. *Science*, 315:1537–1540.

Liou, K. (2002). *An Introduction to Atmospheric Radiation*, page 351. Academic Press.

Lu, Z., Zhang, Q., and Streets, D. (2011). Sulfur dioxide and primary carbonaceous aerosol emissions in china and india, 1996-2010. *Atmospheric Chemistry and Physics*, 11:9389–9864.

Magee (2010). Aethalometer product specifications. `http://www.mageesci.com/images/stories/docs/AE22-31_specSheet_oct2010_rev02_web.pdf`. Accessed: 2014-12-24.

Makynen, M., Cheng, B., and Simila, M. (2013). On the accuracy of thin-ice thickness retrieval using modis thermal imagery over arctic first year ice. *Annals of Glaciology*, 62:87–96.

Matsui, H., Kondo, Y., Moteki, N., Takegawa, N., Sahu, L., Zhao, Y., Fuelberg, H., Sessions, W., Diskin, G., Blake, D., Wisthaler, A., and Koike, M. (2011). Seasonal variation of the transport of black carbon aerosol from the asian continent to the arctic during the arctas aircraft campaign. *Journal of Geophysical Research*, 116:D05202.

McEwen, J. and Johnson, M. (2012). Black carbon particulate matter emission factors for buoyancy driven associated gas flares. *Journal of the Air and Waste Management Association*, 62:307–321.

Mitchell, J. (1957). Visual range in the polar regions with particular reference to the alaskan arctic. *Journal of Atmospheric and Solar-Terrestrial Physics*, Special Supplement:195–211.

NASA (2014a). Aeronet system overview. `aeronet.gsfc.nasa.gov/new_web/system_descriptions.html`. Accessed: 2014-02-24.

NASA (2014b). Modis system specifications. `http://modis.gsfc.nasa.gov/about/specifications.php`. Accessed: 2014-03-27.

NOAA (2009). State of the climate: Wildfires for april 2009. Report.

Park, R., Jacob, D., Chin, M., and Martin, R. (2003). Sources of carbonaceous aerosols over the united states and implications for natural visibility. *Journal of Geophysical Research*, 108:4355.

Park, R., Jacob, D., Yantosca, R., and Chin, M. (2004). Natural and transboundary pollution influences on sulfate-nitrate-ammonium aerosols in the united states: Implications for policy. *Journal of Geophysical Research*, 109:D15204.

Petty, G. (2006). *A first course in atmospheric radiation*, pages 196–202. Sundog Publishing.

Polissar, A., Hopke, P., and Harris, J. (2001). Source regions for atmospheric aerosol measured at barrow alaska. *Environmental Science Technology*, 35:4214–4226.

Pommier, M., Law, K., Clerbaux, C., Turquety, S., Hurtmans, D.and Hadji-Lazaro, J., Coheur, P., Schlager, H., Ancellet, G., Paris, J., Ndlec, P., Diskin, S., Podolske, J., Holloway, J., and Bernath, P. (2010). Iasi carbon monoxide validation over the arctic during polarcat spring and summer campaigns. *Atmospheric Chemistry and Physics*, 10:10655–10678.

Pöschl, U. (2005). Atmospheric aerosols: Comosition, transformation, climate and health effects. *Angewandte Chemie International Edition*, 44:7520–7540.

Qin, Y. and Xie, S. (2012). Spatial and temporal variation of anthropogenic black carbon emissions in china for the period 19802009. *Atmospheric Chemistry and Physics*, 12:48254841.

Quennehen, B., Schwarzenboeck, A., Schmale, J., Schneider, J., Sodemann, H., Stohl, A., Ancellet, G., Crumeyrolle, S., and Law, K. (2011). Physical and chemical properties of pollution aerosol particles transported from north america to greenland as measured during the polarcat summer campaign. *Atmpospheric Chemistry and Physics*, 11:10947–10963.

Quinn, P., Stohl, A., Arneth, A., Berntsen, T., Christensen, J., Flanner, M., Kupiainen, K., Lihavainen, H., Shepherd, M., Shevchenko, V., Skov, H., and Vestreng, V. (2011). *The Impact of Black Carbon on Arctic Climate*, chapter 7. Arctic Monitoring and Assesment Programme.

Rahn, K. and McCaffery (1980). On the origin and transport of the winter arctic aerosol. *Annals of the New York Academy of Sciences*, 338.

Raut, J., Fast, J., Law, K., Weinzierl, B., Rose, M., Kim, J., Thomas, J., and Marelle, L. (2013). Modeling plumes containing black-carbon from siberian sources to the arctic. American Geophysical Union, Fall Meeting 2013.

Remer, L., Kaufman, Y., Tanr, D., Mattoo, S., Chu, D., Martins, J., Li, R., Ichoku, C., Levy, R., Kleidman, R., Eck, T., Vermote, E., and Holben, B. (2004). The modis aerosol algorithm, products, and validation. *Journal of the Atmospheric Sciences*, 62:947–973.

Rienecker, M., Suarez, M., Todling, R., Bacmeister, J., Takacs, L., Liu, H., Gu, W., Sienkieicz, M., Koster, R., Gelaro, R., Stajner, I., and Nielsen, J. (2008). *The GEOS-5 Data Assimilation System Documentation of Versions 5.0.1, 5.1.0, and 5.2.0*. National Aeronautics and Space Administration.

Rignot, E. and Kanagaratnam, P. (2006). Changes in the velocity structure of the greenland ice sheet. *Science*, 311:986–990.

Robertson, J. and Pierce, B. (2008). 90 billion barrels of oil and 1670 trillion cubic feet of natural gas assessed in the arctic. Report.

Rodriguez, E., Toledano, C., Cachorro, V., Ortiz, P., Stebel, K., Berjon, A., Blindheim, S., Gausa, M., and de Frutos, A. (2012). Aerosol characterization at the sub-arctic site andenes by the analysis of columnar optical properties. *Quarterly Journal of the Royal Meteorological Society*, 138:471–482.

Rosen, H., Novakov, T., and Bodhaine, B. (1980). Soot in the arctic. *Atmospheric Environment*, 15:1371–1374.

Sand, M., Berntsen, O., Seland, O., and Kristjansson, J. (2013). Arctic surface temperature change to emissions of black carbon within arctic or midlatitudes. *Journal of Geophysical Research*, 118:7788–7798.

Sandradewi, J., Prvot, A., Weingartner, E., Schmidhauser, R., Gysel, M., and Baltensperger, U. (2008). A study of wood burning and traffic aerosols in an alpine valley using a multi-wavelength aethalometer. *Atmospheric Environment*, 42:101–112.

Schwartz, S. (1996). The whitehouse effect-shortwave radiative forcing of climate by anthropogenic aerosols: An overview. *Journal of Aerosol Science*, 27:359–382.

Seinfeld, J. and Pandis, S. (2006a). *Atmospheric Chemistry and Physics*, page 692. John Wiley and Sons.

Seinfeld, J. and Pandis, S. (2006b). *Atmospheric Chemistry and Physics*, page 109. John Wiley and Sons.

Seinfeld, J. and Pandis, S. (2006c). *Atmospheric Chemistry and Physics*, pages 55–61. John Wiley and Sons.

Serreze, M., Barret, A., and Stroeve, J. (2012). Recent changes in tropospheric water vapour over the arctic as assesed from radiosondes and atmospheric reanalyses. *Journal of Geophysical Research*, 117:D10104.

Sharma, S., Andrews, E., Barrie, L., Ogren, J., and Lavou, D. (2006). Variations and sources of the equivalent black carbon in the high arctic revealed by long-term observations at alert and barrow:1989-2003. *Journal of Geophysical Research: Atmospheres*, 111:D14208.

Sharma, S., Brook, J., Cachier, H., Chow, J., Gaudenzi, A., and Lu, G. (2002). Light absortion and thermal measurements of black carbon in different regions of canada. *Journal of Geophysical Research: Atmospheres*, 107:4771.

Sharma, S., Ishizawa, M., Chan, D., Lavoué, D., Andrews, E., Eleftheriadis, K., and Maksyutov, S. (2013). 16 year simulation of arctic black carbon: Transport, source contribution, and sensitivity analysis on deposition. *Journal of Geophysical Research*, 118:943–964.

Sharma, S., Lavou, D., Cachier, H., Barrie, L., and Gong, S. (2004). Long-term trends of the black carbon concentrations in the canadian arctic. *Journal of Geophysical Research*, 109:D15203.

Shaw, G. (1995). The arctic haze phenomenon. *Bulletin of the American Meteorological Society*, 76:2403–2413.

Shindell, D., Chin, M., Dentener, F., Doherty, R., Faluvegi, G., Fiore, A., Hess, P., Koch, D., MacKenzie, I., Sanderson, M., Schultz, M., Stevenson, D., Teich, H., Textor, C., Wild, O., Bergmann, D., Bey, I., Bian, H., Cuvelier, C., Duncan, B., Folberth, G., Horowitz, L., Jonson, J., Kaminski, J., Marmer, E., Park, R., Pringle, K., Scchroeder, S., Szopa, S., Takemura, T., Zeng, G., Keating, T., and Zuber, A. (2008). A multi-model assessment of pollution transport to the arctic. *Atmospheric Chemistry and Physics*, 8:5353–5372.

Slowik, J., Cross, E., Han, J., Davidovits, P., Onasch, T., Jayne, J., Williams, L., Canagaratna, M., Worsnop, D., Chakrabarty, R., Moosmüller, H., Arnott, W., Schwarz, J., Gao, R., Fahey, D., Kok, G., and Petzold, A. (2007). An intersomparison of instruments measuring black carbon content of soot particles. *Aerosol Science and Technology*, 41.

SRI (2014). Gc detectors: Reduction gas detector. `http://www.srigc.com/RGD.pdf`. Accessed: 2014-05-14.

Stohl, A. (2006). Characteristics of atmospheric transport into the arctic troposphere. *Journal of Geophysical Research*, 111:D11306.

Stohl, A., Kilmont, Z., Eckhardt, S., Kupiainen, K., Shevchenko, V., Kopeikin, V., and Novigatsky, A. (2013). Black carbon in the arctic: the underestimated role of gas flaring and residential combustion emissions. *Atmospheric Chemistry and Physics*, 13:8833–8855.

Stohl, A. and Law, K. (2007). Arctic air pollution: Origins and impacts. *Science*, 315:1537–1540.

Stone, R., Herber, A., Vitale, V., Mazzola, M., Lupi, A., Schnell, R., Dutton, E., Liu, P., Li, S., Dethloff, K., Lampert, A., Ritter, C., Stock, M., Neuber, R., and Maturilli, M. (2010). A three-dimensional characterization of arctic aerosols from airborne sun photometer observations: Pamarcmip april 2009. *Journal of Geophysical Research*, 115:D13203.

Stone, R., Sharma, S., Herber, A., Eleftheriadis, K., and Nelson, D. (2014). A characterization of arctic aerosols on the basis of aerosol optical depth and black carbon measurements. *Elementa*, 2:27.

Stroeve, J., Markus, T., Boisvert, L., Miller, J., and Barret, A. (2014). Changes in arctic melt season and implications for sea ice loss. *Geophysical Research Letters*, 41:1216–1225.

Tomasi, C., Lupi, A., Mazzola, M., Stone, R., Dutton, E., Herber, A., Radinov, V., Holben, B., sorokin, M., Sakerin, S., Terpugova, S., Sobolewski, P., Lanconelli, C., Petkov, B., and Busetto, M. Vitale, V. (2012). An update on polar aerosol optical properties using polar-aod and other measurements performed during the international polar year. *Atmospheric Environment*, 52:29–47.

Trepte, Q., Minnis, P., and Arduini, R. (2003). Daytime and nighttime polar cloud and snow identification using modis data. *SPIE Proceedings*, 4891.

Tschudi, M., Maslanik, J., and Perovich, D. (2008). Derivation of melt pond coverage on arctic sea ice using modis observations. *Remote Sensing of Environment*, 112:2605–2614.

Wang, Q., Jacob, D., Fisher, J., Mao, J., Leibensperger, E., Carouge, C., Le Sager, P., Kondo, Y., Jimenez, J., Cubison, M., and Doherty, S. (2011). Sources of carbonaceous aerosols and deposited black carbon in the arctic in winter-spring: implications for radiative forcing. *Atmospheric Chemistry and Physics*, 11:12453–12473.

Wilkins, E. (1954). Air pollution and the london fog of december 1952. *Journal Royal Sanitary Institute*, 74:1–21.

Zhang, Y., Golaz, J., Deser, C., and Tomas, R. (2011). Climatological characteristics of arctic and antarctic surface-based inversions. *Journal of Climate*, 24:5167–5186.

Zoller, W., Gordon, G., Gladney, E., and Jones, A. (1973). The sources and distribution of vanadium in the atmosphere. *Trace Elements in the Environment*, 1123:31.

Appendix A

Arctic MODIS Evaluation

Another instrument that was evaluated in the Arctic region was the Moderate Resolution Imaging Spectroradiometer (MODIS).

A.1 Instrumentation

There are currently two MODIS instruments orbiting the earth, one on board the Aqua satellite and one on board the Terra satellite. These instruments measure radiation that is reflected or emitted from the surface of the Earth in 36 different bands ranging in wavelength from 0.4 to 14.4 μm. The data that are collected are used for the study of a large number of things such as the altitude and temperature of clouds, the temperature of the Earth's surface, ocean properties, and aerosol properties (NASA, 2014b). A global comparison done using 132 Aerosol Robotic Network (AERONET) sites using AOD at 550 nm found that over land there was a correlation coefficient of 0.8 and a slope of 0.78 between the MODIS retrievals and the measured AERONET AOD, while over the ocean there was a correlation coefficient of 0.91 with a slope of 0.94 (Remer et al., 2004).

The MODIS instrument has been used for a number of different applications in the Arctic. One use is the prediction of sea ice thickness using MODIS ice surface temperature images along with weather data (Makynen et al., 2013), a technique useful for ice up to 50 cm in thickness. Another is the monitoring of melt ponds on top of sea ice using surface reflectance measurements from 3 of the MODIS visible

bands (Tschudi et al., 2008). A third use for MODIS in the Arctic has been the identification of different types of polar clouds and snow for use in the cloud and earth radiant energy system (CERES) which is used to process data for the atmospheric radiation measurements program (Trepte et al., 2003).

The in-situ measurements used for comparison with the MODIS product were Aerosol Robotic Network (AERONET) ground based aerosol measurement sites. These sites are operated by a wide variety of organizations such as universities, national environmental agencies, and individuals. Measurements are taken using a Cimel model 318 sun photometer, which measures the intensity of the Sun's direct beam and the sky at several wavelengths throughout the day at a variety of angles (NASA, 2014a). This data is used to calculate several products including Aerosol Optical Depth (AOD). The data that was used in this research was level 2 data, which is screened for clouds and quality assured. These sites have been used to examine the cycle of AOD in the Arctic, which is different than in other parts of the world. Using data from the Andenes site in Norway, a study found that the annual cycle of aerosols there was much different than at other sites higher in the Arctic. It was found that AOD peaked in May, remaining high through the summer, with low values in the spring (Rodriguez et al., 2012). Conversely, data from Ny Alesund, a station at a similar longitude, but 9.6 degrees of latitude further north, shows the lowest values of AOD occur in the summer and fall, rising rapidly in mid-winter and reaching a maximum in the spring (Herber et al., 2002). This cycle is also observed at Barrow, a site only 2.3 degrees further north but situated in Alaska. A long term analysis of this data has found that in the past decade the peak AOD has been rising, attributed to increasing Eurasian SO_2 emissions (Tomasi et al., 2012).

A.2 Coincident Daily Comparison

The MODIS data used for these comparisons is cloud screened level 2 data from the Terra instrument, which was gridded onto a 0.1° by 0.1° daily average grid. This data was additionally screened by discarding data points with no useful neighbors, and by averaging each point with its nearest neighbors. To evaluate the performance of the MODIS aerosol product in the Arctic, it was compared against the AERONET AOD product in months with a minimum of 4 values. Table A.1 presents the sites that

Site	Latitude	Longitude
Fort McMurray	56.8	-111.48
Yakusk	61.7	129.4
Yellowknife	62.5	-114.4
Kuopio	62.9	27.6
Iqaluit	63.8	-68.5
Bonanza Creek	64.7	-148.3
Andenes	69.3	16.0
Barrow	71.3	-156.7
Resolute Bay	74.7	-94.9
Thule	76.5	-68.8
Hornsund	77.0	15.6
OPAL	80.0	-85.9

Table A.1: Northern AERONET Sites

were used for the comparison. Taken over the entire Arctic, the MODIS instrument shows a reasonable correlation with coincident daily AERONET values, as can be seen in figure A.1. However on a site by site basis, there is much poorer correlation and in general fewer usable points at sites that are further North. This can be seen in figure A.2 which presents daily AOD comparisons at various northern AERONET sites.

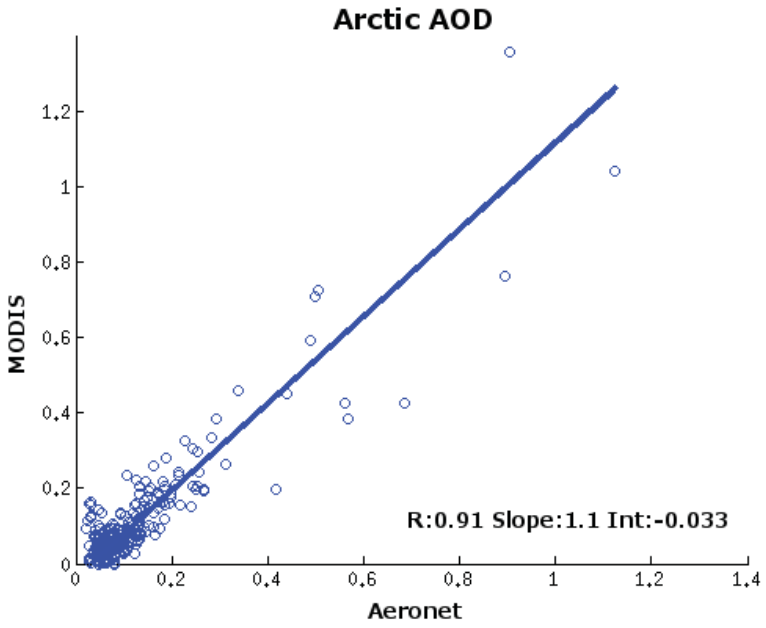

Figure A.1: Coincident Arctic AERONET and MODIS AOD. Fit line is calculated using reduced major axis regression

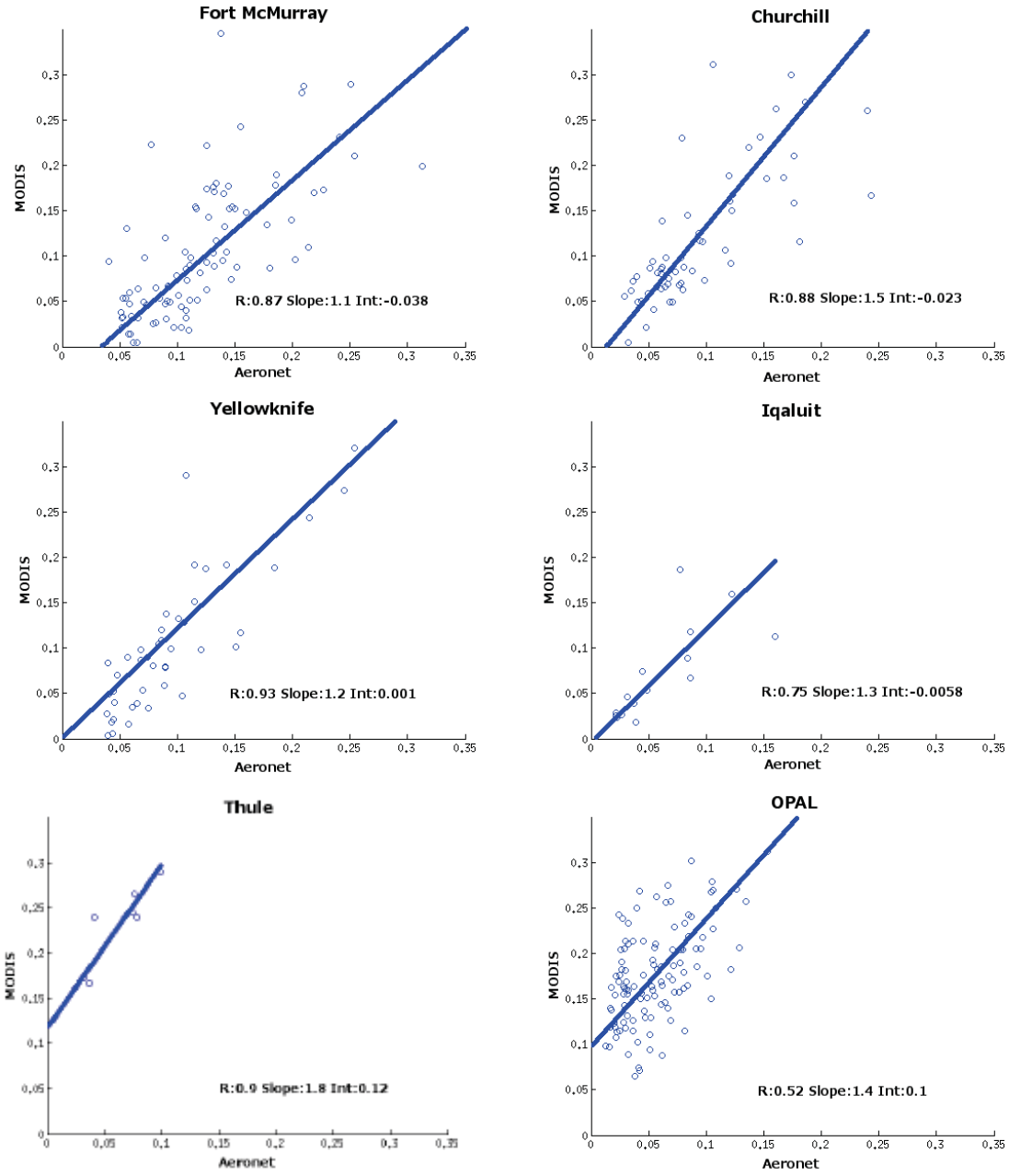

Figure A.2: Comparison of daily AERONET and coincident MODIS AOD at selected arctic and subarctic sites. Fit lines are calculated using reduced major axis regression.

A.3 Monthly Average Comparisons

In addition to comparing coincident daily measurements, long term averages were considered as well which were made from all available data. This was done as the cloud filtering that is gained by only using coincident AERONET and MODIS points is limited to when AERONET is available, and in the locations of AERONET stations. These comparisons produced results similar to what was observed from the coincident daily comparisons. Figure A.3 shows a reasonable correlation over the Arctic, however once again when examined on a station by station basis, the quality is highly variable, as can be seen in figure A.4. Figure A.5 shows an average of MODIS data during the summer months of 2008-2011, along with Arctic AERONET sites during the same period. From this map we can see the amount of noise in the data, with no real pattern or realistic distribution, and the AOD values reported by MODIS do not match what is seen at the AERONET sites.

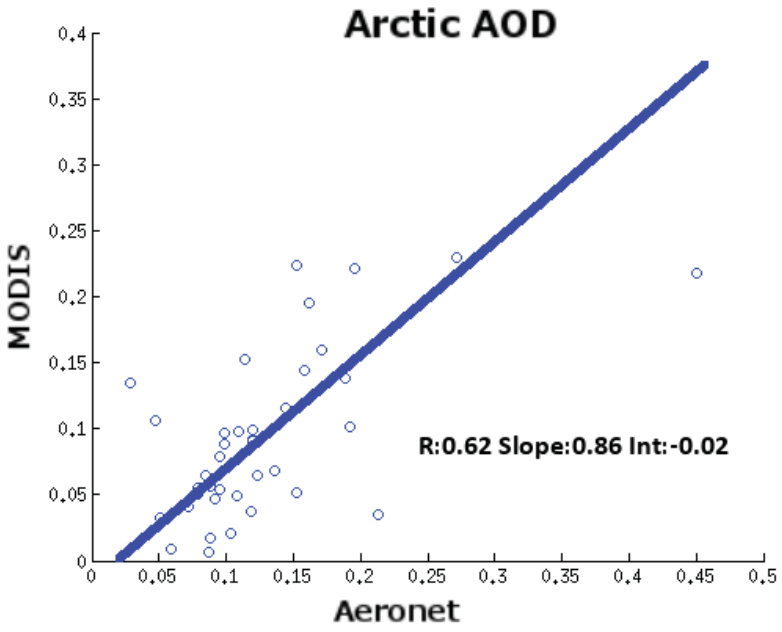

Figure A.3: Comparison of monthly average AERONET and MODIS AOD from arctic and subarctic sites.

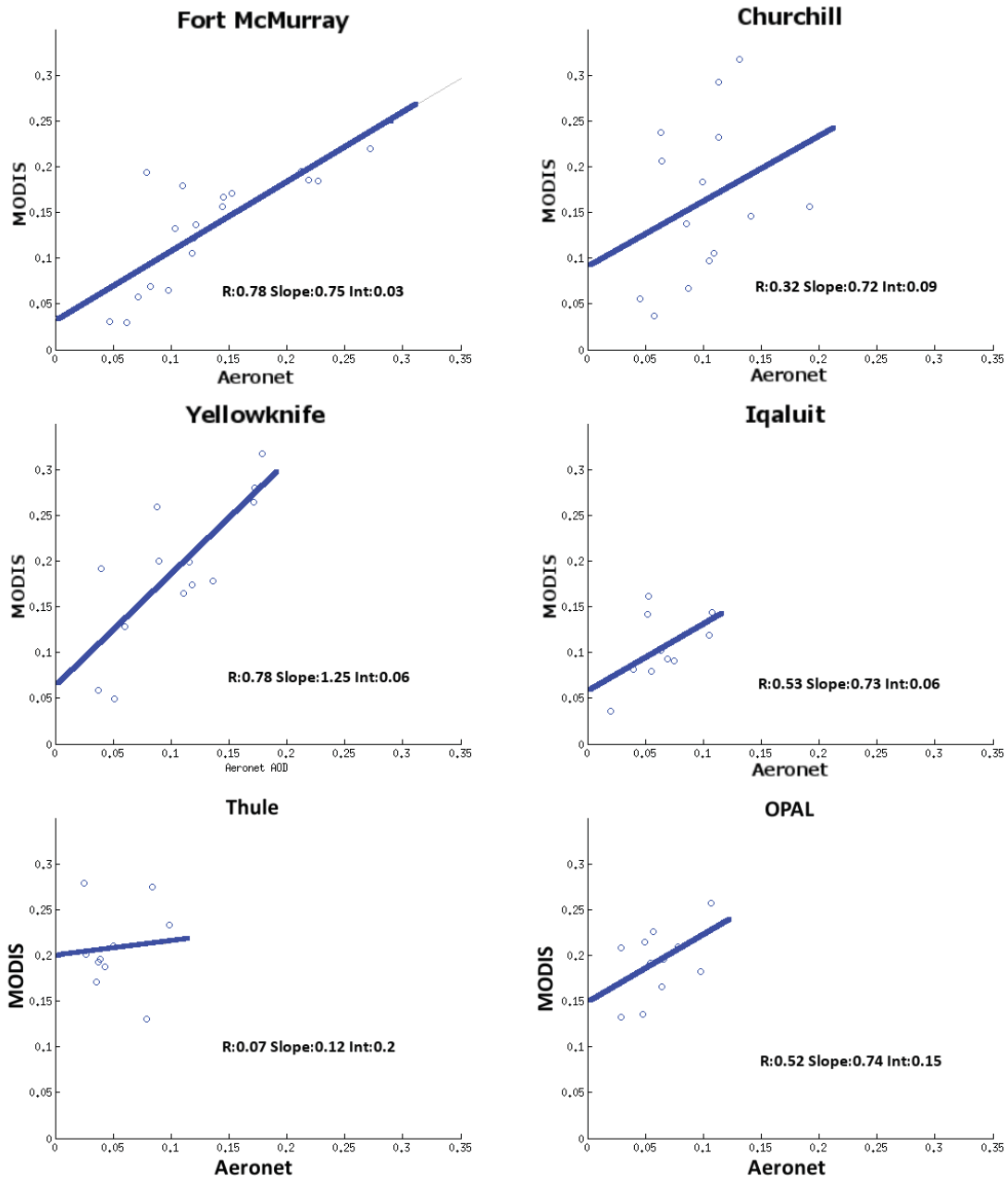

Figure A.4: Comparison of monthly AERONET and MODIS AOD at selected arctic and subarctic sites. Fit lines are calculated using reduced major axis regression.

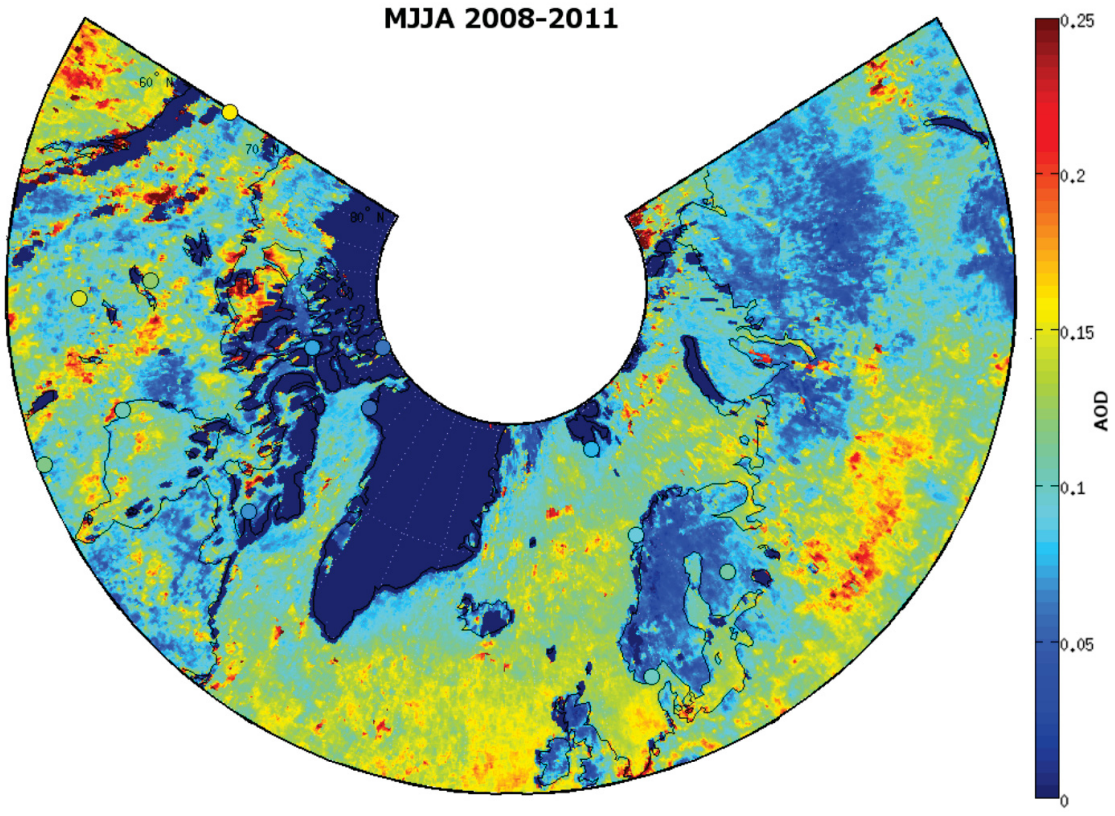

Figure A.5: Average Arctic MODIS AOD during summer months 2008 to 2011. AERONET site averages are shown during the same time period in filled circles.

A.4 Conclusions

There are several possible causes for the poor quality of this dataset in the Arctic. The MODIS aerosol product relies upon reflected radiation from the sun, and the Arctic is covered by highly reflective snow and ice for a large part of the year. This can cause problems for the aerosol retrieval algorithm as it was designed for darker surfaces. Another possible cause is that solar zenith angles in the Arctic are high, which causes some data to be discarded as the algorithm can only use points with solar zenith angles that are less than 75 degrees. The reason for the evaluation of this data set was the longevity of the MODIS instruments, with data available from 1999 for the Terra instrument and 2002 for the Aqua instrument, along with successful applications to other Arctic research questions as discussed earlier. Unfortunately there was too much uncertainty in the data for what we wanted to accomplish, and as such it was decided not to pursue the use of this dataset.